Remote Sens. **2015**, *7*, 4391-4423; doi:10.3390/rs70404391

OPEN ACCESS

remote sensing

ISSN 2072-4292

www.mdpi.com/journal/remotesensing

Article

Drought Variability and Land Degradation in Semiarid Regions: Assessment Using Remote Sensing Data and Drought Indices (1982–2011)

Sergio M. Vicente-Serrano [1,*], Daniel Cabello [2,3], Miquel Tomás-Burguera [4], Natalia Martín-Hernández [1], Santiago Beguería [4], Cesar Azorin-Molina [1] and Ahmed El Kenawy [5,6]

1 Instituto Pirenaico de Ecología, Spanish National Research Council (IPE-CSIC), Campus de Aula Dei, P.O. Box 13034, E-50059 Zaragoza, Spain; E-Mails: nmartin@ipe.csic.es (N.M.-H.); cazorin@ipe.csic.es (C.A.-M.)

2 Department of Economy, University of Alcala, E-28801 Madrid, Spain; E-Mail: d.cabello@edu.uah.es

3 Madrid Institute for Advanced Studies in Water (IMDEA-Water), Alcalá de Henares, E-28805 Madrid, Spain.

4 Estación Experimental de Aula Dei, Spanish National Research Council (EEAD-CSIC), Campus de Aula Dei, P.O. Box 13034, E-50059 Zaragoza, Spain; E-Mails: mtomas@eead.csic.es (M.T.-B.); sbegueria@eead.cis.es (S.B.)

5 Hydrological Modeling & Earth Observation Group, WDRC, King Abdullah University of Science and Technology, 23955-6900 Thuwal, Saudi Arabia; E-Mail: kenawy@mans.edu.eg

6 Department of Geography, Mansoura University, 35516 Mansoura, Egypt

* Author to whom correspondence should be addressed; E-Mail: svicen@ipe.csic.es.

Academic Editors: Arnon Karnieli, Soe Myint and Prasad S. Thenkabail

Received: 25 December 2014 / Accepted: 1 April 2015 / Published: 14 April 2015

Abstract: We analyzed potential land degradation processes in semiarid regions worldwide using long time series of remote sensing images and the Normalized Difference Vegetation Index (NDVI) for the period 1981 to 2011. The objectives of the study were to identify semiarid regions showing a marked decrease in potential vegetation activity, indicative of the occurrence of land degradation processes, and to assess the possible influence of the observed drought trends quantified using the Standardized Precipitation Evapotranspiration Index (SPEI). We found that the NDVI values recorded during the period of maximum vegetation activity ($NDVI_{max}$) predominantly showed a positive

evolution in the majority of the semiarid regions assessed, but $NDVI_{max}$ was highly correlated with drought variability, and the trends of drought events influenced trends in $NDVI_{max}$ at the global scale. The semiarid regions that showed most increase in $NDVI_{max}$ (the Sahel, northern Australia, South Africa) were characterized by a clear positive trend in the SPEI values, indicative of conditions of greater humidity and lesser drought conditions. While changes in drought severity may be an important driver of NDVI trends and land degradation processes in semiarid regions worldwide, drought did not apparently explain some of the observed changes in $NDVI_{max}$. This reflects the complexity of vegetation activity processes in the world's semiarid regions, and the difficulty of defining a universal response to drought in these regions, where a number of factors (natural and anthropogenic) may also affect on land degradation.

Keywords: Standardized Precipitation Evapotranspiration Index (SPEI); NDVI; NOAA-AVHRR; GIMMS; desertification; vegetation recovery

1. Introduction

Semiarid vegetation is well adapted to long periods of water scarcity, through various phenological and morphological mechanisms [1]. Under natural conditions, semiarid vegetation should not be severely damaged by extreme drought events because it is markedly resilient and has the capacity to recover. Nevertheless, the majority of semiarid regions worldwide is subject to anthropogenic perturbations, and is far from the natural equilibrium state. As a consequence of anthropogenic climate forcing and intensive historical land uses (e.g., grazing, agriculture, etc.), semiarid regions are prone to land degradation processes. Climate and human forcing can trigger positive feedback between the biota and the physical environment, leading the ecosystem towards a degraded state; if taken beyond a threshold, return to the initial state is very difficult [2–5].

Current climate change processes have been recognized as important factors in land degradation [6–8]. Global warming can affect precipitation seasonality and magnitude [9], but may also affect land surface water balances through changes in the atmospheric evaporative demand (AED), which will probably increase in coming decades as a response to increased air temperature and increased vapor pressure deficit [10]. It is expected that climate change will make droughts more frequent and severe in the future [11], which may continue current land degradation and trigger new processes in semi-arid regions.

Drought has been considered to be a major factor triggering land degradation processes, and studies have stressed the importance of drought episodes in explaining the occurrence of major degradation in some regions [12,13]. Nevertheless, the scientific debate about these issues is not resolved. Some studies have argued that drought cannot be a factor explaining degradation trends, given the common resilience of semiarid vegetation communities and the general recovery of the vegetation following an increase in precipitation, even after long dry periods including those recorded in past decades in the Sahel [14,15]. Thus, global studies suggest that the world's semiarid regions have shown a greater increase in vegetation activity than that observed for water availability [16]. Nevertheless, some

studies have shown that in semiarid regions characterized by soil limitations and intense human pressure, drought intensification as a consequence of warming processes may trigger land degradation processes [17]. These may be irreversible in areas in which edaphic conditions markedly limit vegetation establishment and development [18,19], even with the application of ecological restoration practices [20].

A number of studies have analyzed vegetation dynamics in response to climate variability [21–24], but very few have analyzed the response to drought through accurate quantification of drought severity using drought indices [25–29]. In general, these studies have shown that although semiarid vegetation is usually resistant and highly resilient to water deficits, vegetation activity in semiarid regions is highly controlled by interannual variations in water availability [30], and a decrease in water availability may trigger land degradation [12].

Remote sensing data provide a global long-term overview of the vegetation dynamics, and complement more detailed ground studies. In combination with analysis of other socioeconomic and biophysical variables, these data may enable greater understanding of land degradation mechanisms and the consequences of drought evolution and severity on land degradation. Studies based on available time series of remote sensing images and gridded climate databases have reported degradation processes in some regions that could be associated with changes in drought frequency and severity [12], but may also be influenced by human land management practices [31,32]. Nevertheless, the complexity of the response of global ecosystems to drought severity involves the various vegetation strategies [33], but also the drought magnitude and particularly the time scale at which the drought severity is measured [30]. This makes it difficult to assess the possible influence of drought on current land degradation processes. Although some studies have analyzed vegetation activity trends and possible degradation processes in semiarid regions using remote sensing data [16,34,35], the effect of drought severity has not been considered in these analyses. The current scientific debate about the surface extent and severity of desertification in semiarid lands, and how these are influenced by drought variability and trends [36], makes studies in this area a priority under current climate change scenarios.

In this study we investigated land degradation processes in the world's semiarid regions, measured using long time series of remote sensing images. The objectives of the study were to identify semiarid regions showing a marked decrease in the annual maximum vegetation activity, which could be indicative of the occurrence of land degradation processes, and to determine the possible influence of the observed drought trends. We used a multi-scalar drought index, the Standardized Precipitation Evapotranspiration Index (SPEI), which accounts for the positive influence of precipitation and the negative influence of the AED on drought severity. The SPEI is likely to be better than other indices for assessing the varying sensitivity of vegetation communities to water deficits [37], as it can be obtained on different time scales [38].

2. Data and Methods

2.1. Datasets

2.1.1. Global Normalized Difference Vegetation Index

Various remote sensing products enable the assessment of vegetation variability and change at the global scale. The datasets derived from SPOT (*Satellite Pour l'Observation de la Terre*)-Vegetation, MODIS (Moderate-Resolution Image Spectroradiometer)-Aqua and Terra satellites each provide the Normalized Difference Vegetation Index (NDVI) from 1998 and 2000 but currently the unique earth observation program, which currently enables analysis of vegetation activity over the past three decades, is provided by the National Oceanic and Atmospheric Administration (NOAA) Polar orbiting satellites. The NOAA satellites contain the Advanced Very High Resolution Radiometer (AVHRR) sensor, which collects spectral information in the visible and near infrared regions, facilitating calculation of the NDVI [39]. The NDVI data from NOAA-AVHRR sensors have been widely used to analyze vegetation variability and trends in various regions of the world [16,40–42]. A range of NDVI global datasets have been developed from NOAA-AVHRR. Beck *et al.* [43] conducted a review of the available datasets and their performance in spatial and temporal studies. Currently, the most widely used global dataset of NDVI from NOAA-AVHRR data is the Global Inventory Monitoring and Mapping Studies (GIMMS) database [44], which covers a longer period than the other available datasets (1981–2011). The GIMMS NDVI data is generated from the original 1.1 km^2 NOAA-AVHRR data as bi-weekly maximum value composites aggregated to an 8 × 8 km pixel resolution. The quality and consistency of the GIMMS data are assured by correction for (i) sensor degradation, (ii) sensor intercalibration differences, (iii) solar zenith and viewing angles, (iv) volcanic aerosols, (v) atmospheric water vapor, and (vi) cloud cover. By comparing NOAA GIMMS and Landsat images, Beck *et al.* [43] showed that the GIMMS is the most accurate AVHRR-NDVI dataset for assessing vegetation variability and trends. A recent Special Issue of the journal Remote Sensing has focused on the description and applications of the third generation (3g) GIMMS NDVI. This issue includes a detailed description of the dataset [45], and studies on climate impacts on vegetation [46–48], vegetation trends [49–52] and land degradation in certain regions of the world [53,54]. In this study we used the GIMMS NDVI3g at a spatial resolution of 0.083° with a 15-day temporal interval for the period of July 1981 and December 2011. To enable comparison with existing drought datasets, these data were transformed to monthly values using the Maximum Value Composite of the two monthly 15-day images.

2.1.2. Drought Data

To assess global scale drought variability for the period 1981–2011 we used the SPEIbase [55], which is based on the SPEI [38]. The SPEI is obtained from the monthly climatic water balance (precipitation minus reference evapotranspiration (ETo-)), which is adjusted using a three-parameter log-logistic distribution. The values are accumulated at various time scales and converted to standard deviations with respect to average values. The SPEI has clear advantages over other drought indices as it facilitates better spatial comparability [56], has greater capacity than other drought indices to identify

drought impacts in a variety of systems [37], and has more coherent response to precipitation and the AED than other indices [57]. We used SPEI time scales from 1 to 12 months. Although the vegetation of some regions may respond to longer time scales, semiarid vegetation mostly responds to drought time scales <6 months [30]. The monthly 0.5° spatial resolution SPEI was transformed to 8 km to match the GIMMS NDVI3g data, using a bilinear convolution. Although this approach could introduce inaccuracies when applied in areas having complex topography and marked climate variability, most of the semiarid regions identified in this study correspond to areas of plain having minor topographic variation and little climate variability. Consequently, it was assumed that the change of resolution of the climate dataset would have minor effects on the resulting analysis.

2.1.3. Other Data

We also used other auxiliary global datasets to identify the study domain. Thus, we used a global land cover map (GlobCover) to select regions suitable for analysis based on the land cover type. GlobCover is a European Space Agency initiative to develop a global land cover map using input observations from the 300m MERIS sensor on board the ENVISAT satellite mission. To match the GIMMS NDVI3g data, these satellite data were also transformed to 8 km resolution using a mode filter, with land cover categories being assigned according to the mode of the 300 m cells contained within each 8-km cell. We also used global records of annual precipitation and annual reference evapotranspiration from the Climate Research Unit (CRU) TS3.2 dataset [58]. This is the most complete and updated dataset of gridded precipitation and reference evaporation at the global scale. It has a spatial resolution of 0.5°, and covers the period 1901–2013. The maps of annual precipitation and ETo at a resolution of 0.5° were also transformed to 8 km using the bilinear convolution approach referred to above.

2.2. Analysis

2.2.1. Identification of Semiarid Regions

We firstly identified the semiarid regions of the world using annual precipitation and the ETo climatology. Various approaches have been used to identify the world's semiarid regions [59,60]. These are based on values of precipitation and the AED. The United Nations Environmnet Programme [61] proposed an indicator based on the quotient between precipitation and AED; but this diminishes the role of the AED in relation to precipitation in determining water deficit conditions [57]. We calculated a simple climatic water balance based on the difference between the average annual precipitation and the average ETo, which quantifies the available deficit or surplus of water at each site. After testing various thresholds we identified semiarid regions according to a threshold of $P - ETo = -200$ mm year^{-1}, as this provides a better match with current semiarid vegetation biomes [62]. In these regions we selected the natural vegetation areas from the GlobCover dataset, and removed deserts, human infrastructure, urban areas and cultivated lands. Most of the selected lands correspond to areas of herbaceous and shrubs cover. Figure 1 shows the spatial distribution of the semiarid regions according to these criteria.

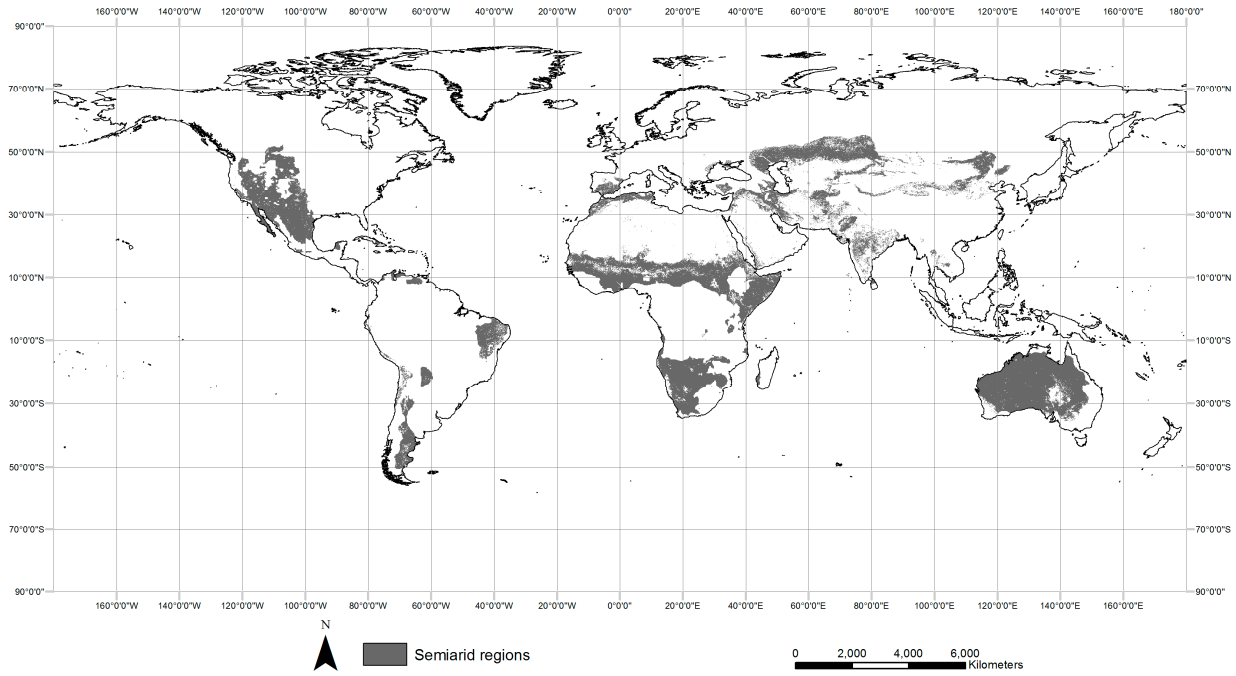

Figure 1. Spatial distribution of the semiarid regions analyzed in the study.

2.2.2. Identification of the Month of Maximum Vegetation Activity ($NDVI_{max}$)

Land degradation is usually described as the loss of potential productivity in a vegetation community [2,63]. Vegetation productivity is usually assessed using satellite images integrated over biweekly or monthly periods during the active period [64–66]. Nevertheless, an annual parameter is not suitable for identifying land degradation processes, as a loss of productivity over the period in which the maximum is recorded could be masked by changes during periods of growth or senescence. Moreover, vegetation activity can respond differently to drought conditions, as a function of seasonality [29]. In addition, using an annual summary of vegetation activity does not allow defining the SPEI drought time scales that are affecting the NDVI in the various months of the year. Consequently, we analyzed land degradation taking into account the month at which maximum vegetation activity was recorded, which varied among the semiarid regions analyzed. The $NDVI_{max}$ provided information on the maximum potential vegetation activity in each region, and although it may not be fully indicative of all annual vegetation growth, and the month corresponding to this value can change from year to year; we have found a strong one-month autocorrelation in the monthly NDVI series of most of the analyzed semiarid regions and also a high correlation between the $NDVI_{max}$ and the annual integrated NDVI (results not shown). This reduces shortcomings in the methodology used. The month in which maximum vegetation activity was recorded in each 8-km pixel was identified using the monthly average NDVI values over the 30 years for which data were available, selecting the month in which monthly averages corresponded to the annual maximum NDVI. Figure 2 shows the month of the year in which the maximum value NDVI was reached in each region.

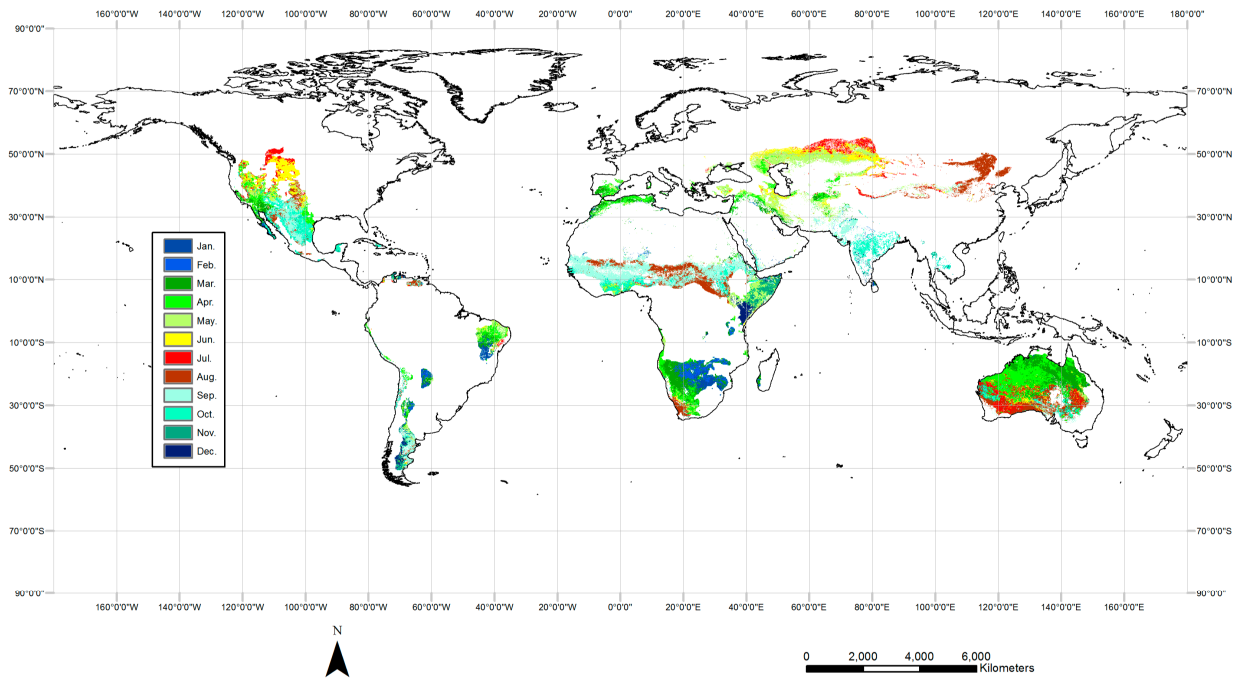

Figure 2. Month of the year in which the monthly average maximum Normalized Difference Vegetation Index ($NDVI_{max}$) was recorded.

2.2.3. $NDVI_{max}$ Trends: Sign and Magnitude

We firstly analyzed the NDVI trends in the months of average maximum vegetation activity. For this purpose we selected the monthly series of the NDVI corresponding to the month of average monthly maximum NDVI ($NDVI_{max}$). The Mann-Kendall statistical test was used to determine trend significance. The nonparametric coefficient (Mann-Kendall tau) was selected because it is more robust than parametric coefficients, and does not assume normality of the data series [67]. The value of tau measures the degree to which a trend is consistently increasing or decreasing. In our study positive values of tau indicated a trend of increasing vegetation cover, and negative values indicated decreasing cover. Statistically significant trends were defined as those below the threshold $p < 0.1$. We also analyzed the magnitude of change in $NDVI_{max}$. To identify areas that underwent the greatest changes in $NDVI_{max}$ we used a regression analysis between the series of time (independent variable) and the temporal $NDVI_{max}$ (dependent variable). The results yielded one model for each 8-km grid, and took the form $y = mx + b$. The slope of each model (m) indicated the change in $NDVI_{max}$ per year, which we multiplied by 10 to provide a more comprehensive measurement of $NDVI_{max}$ change decade^{-1}.

2.2.4. Time Scale of SPEI with Maximum Correlation between $NDVI_{max}$ and SPEI

We secondly analyzed the existing correlation between the $NDVI_{max}$ and SPEI in each 8-km grid cell. As noted above, the response of vegetation to drought can differ as a function of the drought time scale [30]. As a consequence of different physiological, anatomical or edaphic factors, some vegetation communities can show a response to short periods of water deficit, whereas others may be resistant to soil water deficit and/or enhanced AED, and respond to longer drought time scales representative of water deficits of longer duration. As it was not possible to know *a priori* how the $NDVI_{max}$ responded

to SPEI time scales in each grid cell, we correlated $NDVI_{max}$ with the 1- to 12-month SPEI series for the same month, and retained maximum correlation for further analysis. Figure 3 illustrates this procedure. The plots to the left show the monthly evolution of the 1-, 3- and 12-month SPEI and $NDVI_{max}$ for 28.7°S, 23.1°E. The plots to the right show the evolution of $NDVI_{max}$ in the month of average maximum NDVI and the evolution of the 3-, 6- and 12-month SPEI. It shows that the $NDVI_{max}$ mainly relates to cumulative water deficits at shorter time scales, reaching a maximum correlation with the 3-month SPEI, which was selected for the analysis for this location. Significant correlations between the $NDVI_{max}$ and SPEI were based on a threshold of $p < 0.1$.

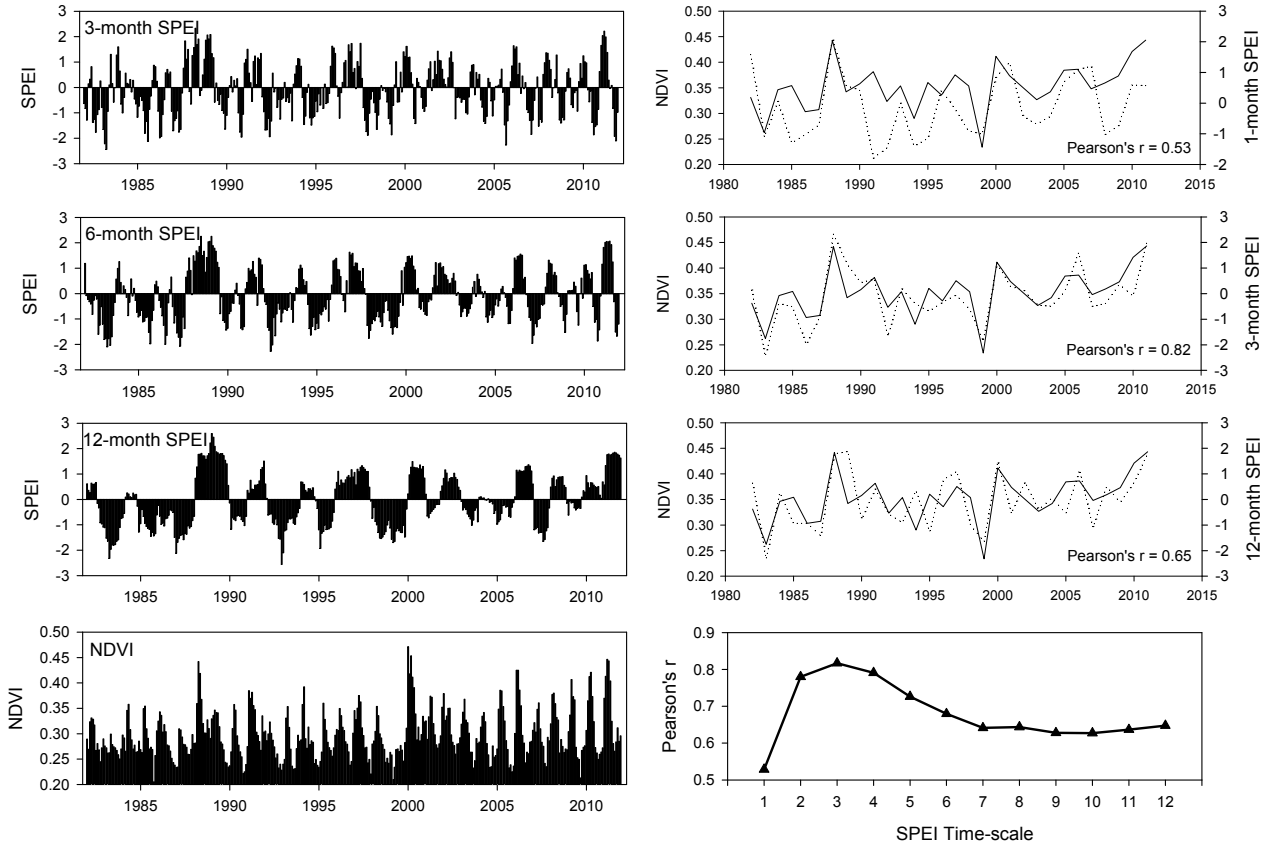

Figure 3. Example of the analysis used to determine the influence of various drought time-scales on the maximum NDVI at 23.1°E, 28.7°S. The left column shows the evolution of the 3-, 6- and 12-month Standardized Precipitation Evapotranspiration Index (SPEI) and the monthly NDVI. The right column shows the evolution of the NDVI (solid line) and the 1-, 3- and 12-month SPEI (dotted line) during the month in which the average maximum NDVI was recorded. The bottom plot shows the correlation between the NDVI and the 1- to 12-month SPEI.

2.2.5. Relationship between $NDVI_{max}$ Trends and SPEI Trends

To identify possible relationships between observed trends in the $NDVI_{max}$ and changes in drought severity, we also assessed (Mann-Kendall tau test; $p < 0.1$) the trends in the SPEI series for each 8-km grid cell corresponding to the month of $NDVI_{max}$ and the SPEI time scale at which the maximum correlation between $NDVI_{max}$ and SPEI was reached. The magnitude of change in the SPEI was also

assessed using least-square simple regression between the series of time (as independent variable) and the series of the SPEI. To detect any association between the observed changes in $NDVI_{max}$ and SPEI we related the observed $NDVI_{max}$ changes (in NDVI units per decade) between 1981 and 2011 to the SPEI changes (in SPEI units per decade). Moreover, we related the sign and the signification of the trend in both the NDVI and SPEI using a cross tabulation analysis [68]. This assesses the spatial distributions of trend signs (positive and significant, positive but non-significant, negative and significant, negative but non-significant) between $NDVI_{max}$ and the SPEI. Thus, the default structure of the table was 4 × 4. This enabled similarities among the spatial distributions of the NDVI and SPEI to be detected. Statistical assessment of the overlaps was based on the chi-squared (χ^2) test. The null hypothesis (H0) was that the spatial distribution of the two categorical variables was independent and randomly distributed. The alternative hypothesis (H1) was that the spatial association between the two categorical variables was significant. When the null hypothesis is rejected, the degree to which the categorical variables are associated can be calculated using the coefficient of contingency [69], which can be interpreted using the Pearson's *r* statistic.

2.2.6. Regression Model $NDVI_{max}$-SPEI

Finally, following a methodology similar to that proposed by Evans and Geerken [31], and used extensively [32,70–72], we calculated a regression model for each 8-km grid cell in which a significant correlation between the SPEI and NDVI was found. The SPEI of the month of $NDVI_{max}$ and the time scale of strongest $NDVI_{max}$ -SPEI correlation was the independent variable, and the $NDVI_{max}$ was the dependent variable. To focus on the regions in which the $NDVI_{max}$ variability was related to drought change, we selected only those grid cells in which a significant correlation was found between both variables. This enabled a residual per year (the difference between the observed $NDVI_{max}$ and the modeled $NDVI_{max}$ by SPEI) to be obtained. We are aware that the SPEI does not comprise all effects of meteorology on plant growth. For instance, precipitation intensity is a factor, which is not considered by current drought indices and it could be highly relevant to explain soil water availability in semiarid regions. Moreover, other atmospheric phenomena such as heat waves, frost periods, *etc.*, are also not well captured by drought indices. Nevertheless, in world semiarid regions, the main limiting factor for the vegetation growth is the soil water availability, which is driven by two main elements: (i) the total precipitation recorded over a certain period of time, and (ii) the atmospheric evaporative demand (AED). These two variables are considered in the SPEI, taking into account the influence of the incoming solar radiation and temperature but also relative humidity and wind speed on the NDVI by means of their inclusion in the reference evapotranspiration calculations.

Trend analysis was also applied to the residual series using the Mann-Kendall test and the magnitude of the trend, assessed using simple regression models. The evolution of these residual series may be indicative of: (i) an increase of the $NDVI_{max}$ above the expected potential according to the evolution of drought conditions (*i.e.*, a positive trend of residuals), which could be indicative of decreased perturbations affecting the ecosystem (e.g., human pressure); (ii) a stationary evolution in which the residuals do not show any trend, and the evolution of the $NDVI_{max}$ follows the evolution of water availability according to the SPEI evolution; and (iii) a decrease of the $NDVI_{max}$ below the expected potential according to the SPEI evolution (a negative evolution of the residuals), which could

be indicative of a lesser increase in the $NDVI_{max}$, or a larger decrease in $NDVI_{max}$ than expected according to the SPEI evolution.

To identify factors that might drive the observed evolution of the $NDVI_{max}$, the spatial patterns of correlation between the SPEI and $NDVI_{max}$ and the evolution of the series of residuals were related to the sign and significance of correlations (between the SPEI and $NDVI_{max}$) or trends (for the $NDVI_{max}$, SPEI and the series of residuals) (positive and significant, positive and non-significant, negative and significant and negative and non-significant) and with the average $NDVI_{max}$ and the average aridity index (see Section 2.2.1). The sign and signification of the series of residuals were also related to the observed change in the SPEI and $NDVI_{max}$. We also considered the Water Use Efficiency (WUE) [73] for each 8-km grid cell; this is a parameter similar to the Rainfall Use Efficiency (RUE). The RUE is a standard measure widely used to assess the health of ecosystems and their productive capacity [2,71,74]. The WUE was estimated as the quotient between the average annual climatic water balance (the difference between precipitation and ETo, plus a constant to ensure positive values) and the average maximum NDVI. We judged that WUE may be more useful than the RUE for quantifying the efficiency of use of the available water, as it takes into account both precipitation and the AED. Lower values of WUE are indicative of a decreased capacity for generating green biomass per unit of available water, and usually represent more degraded areas [2,74,75]. We compared graphically the values of these variables in each of the four trend groups, and assessed the statistical differences among the groups using one-way analysis of variance (ANOVA). We used the Tamhane *post-hoc* contrast to identify subsets of means that do not differ from each other. This test uses the Student's *t* distribution and it is appropriate even when variances and group sizes are unequal. In other words, it does not require the assumption of homogeneity in the variance of the factors among the trend groups, and here it was used to identify the statistically significant differences among the trend groups for each of the variables.

3. Results

3.1. $NDVI_{max}$ Trends

Figure 4 shows the spatial distribution of changes in the $NDVI_{max}$ during the month of maximum vegetation activity in the semiarid regions of the world. Figure 5 shows the percent of semiarid regions with positive and negative changes, and the magnitude of the changes observed. Positive trends clearly dominated across the world's semiarid regions for the period 1982–2011. More than 70% of the regions showed a positive trend in $NDVI_{max}$, 30% of which were significant, while for only 5% of the semiarid zones was there a significant negative trend (see Figure 5). Large areas showed clear significant positive trends (including amongst others the Sahel; northwest India; northeast Australia; the northwestern border area of South Africa with Botswana, Zimbabwe and Mozambique; southeast of the Iberian Peninsula; central and southeastern areas of North America). Other areas of smaller extent showed significant negative trends (a band through central Asia extending west to east, the interior of the Horn of Africa, California, north of Patagonia). Therefore, the dominant pattern at the global scale showed a general $NDVI_{max}$ increase throughout the world's semiarid regions.

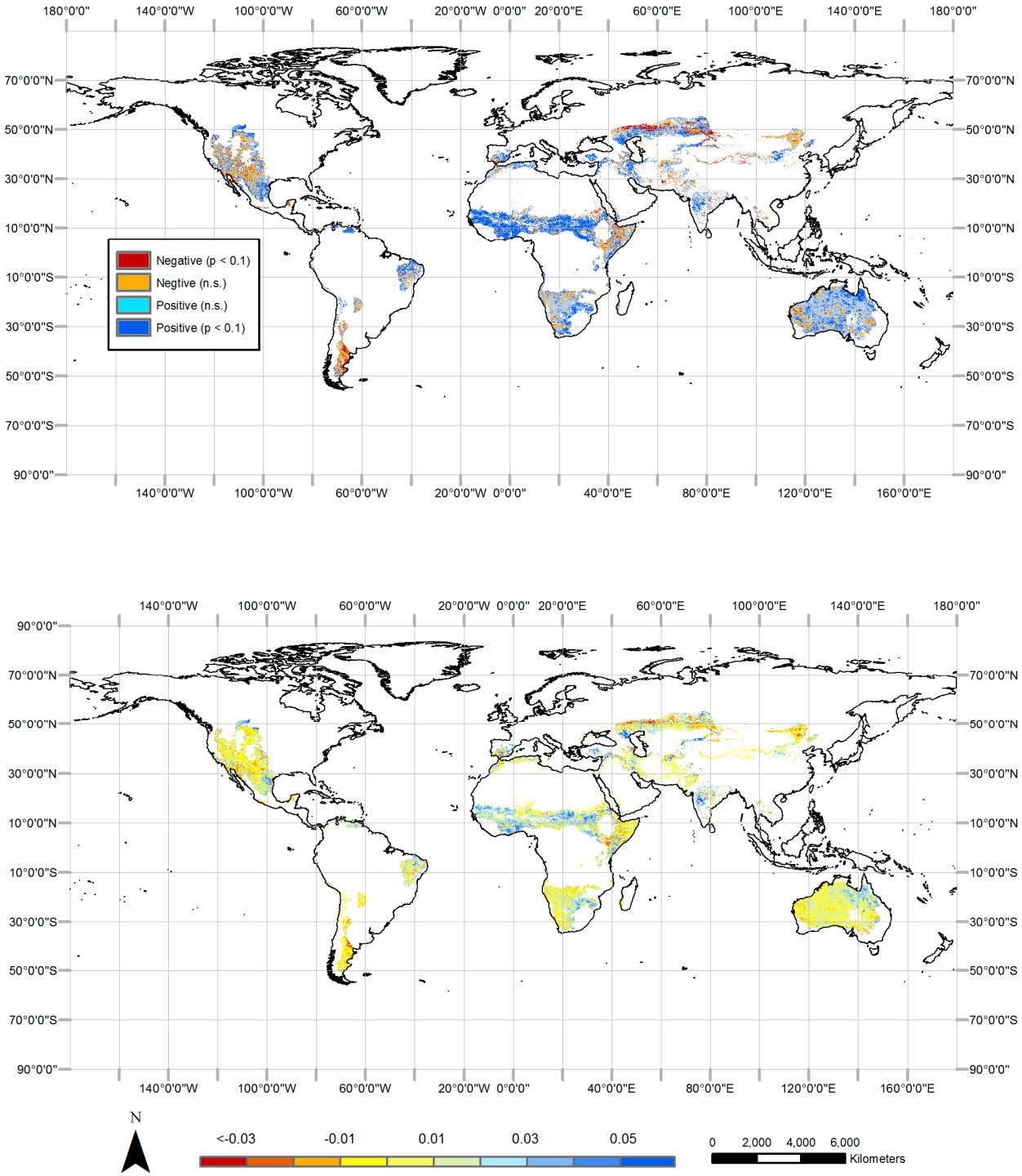

Figure 4. Trends in the NDVI in semiarid regions during the month of average maximum vegetation activity, under the assumption of monotonic change (1982–2011). Top: sign and signification ($p < 0.1$) of the trends. Bottom: magnitude of the trend (in NDVI units decade^{-1}).

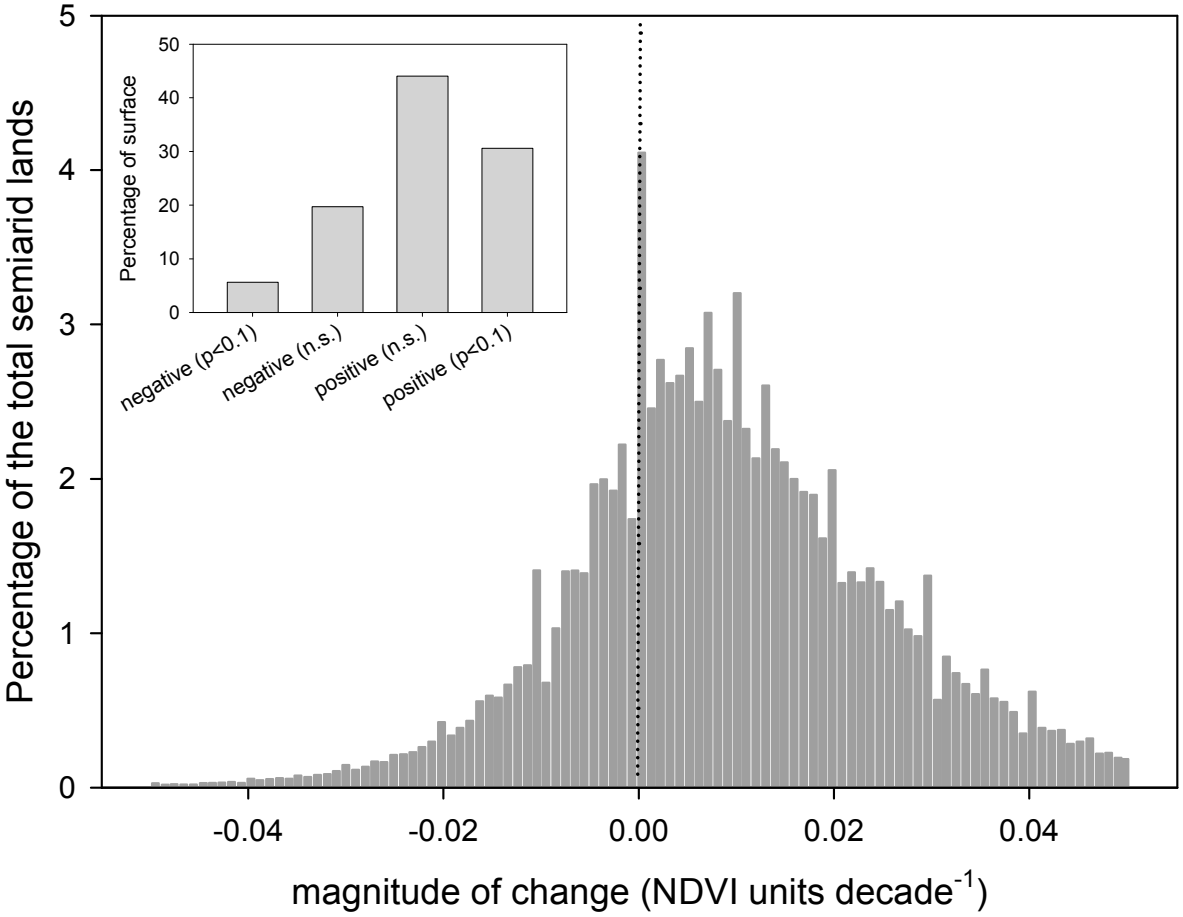

Figure 5. Percentage of semiarid lands according to the observed NDVI magnitude of change (NDVI units decade^{-1}) between 1982 and 2011. The inset graph shows the percentages of semiarid lands having negative and positive trends (including signification).

Figure 6 provides a box plot showing the values of average $NDVI_{max}$, climate aridity and WUE as a function of the four categories of $NDVI_{max}$ trend. The positive and significant trends correspond to areas that showed higher average $NDVI_{max}$ and WUE values than the other trend categories. Nevertheless, only the areas having positive and significant trends showed statistically significant differences from the other trend categories. In contrast, the various trend categories showed a clear difference in aridity values (annual precipitation minus annual ETo). In general, the areas showing negative and significant trends in $NDVI_{max}$ mostly corresponded to areas associated with lower climate aridity, whereas the areas showing positive and significant $NDVI_{max}$ trends in general corresponded to the most arid regions, although this pattern could have little validity on a local scale. The differences in the average aridity between the various groups of $NDVI_{max}$ trends were statistically significant, according to the ANOVA analysis and the Tamhane *post-hoc* test at $p < 0.001$, which suggests that the observed trends in $NDVI_{max}$ between 1982 and 2011 were controlled by spatial patterns in aridity.

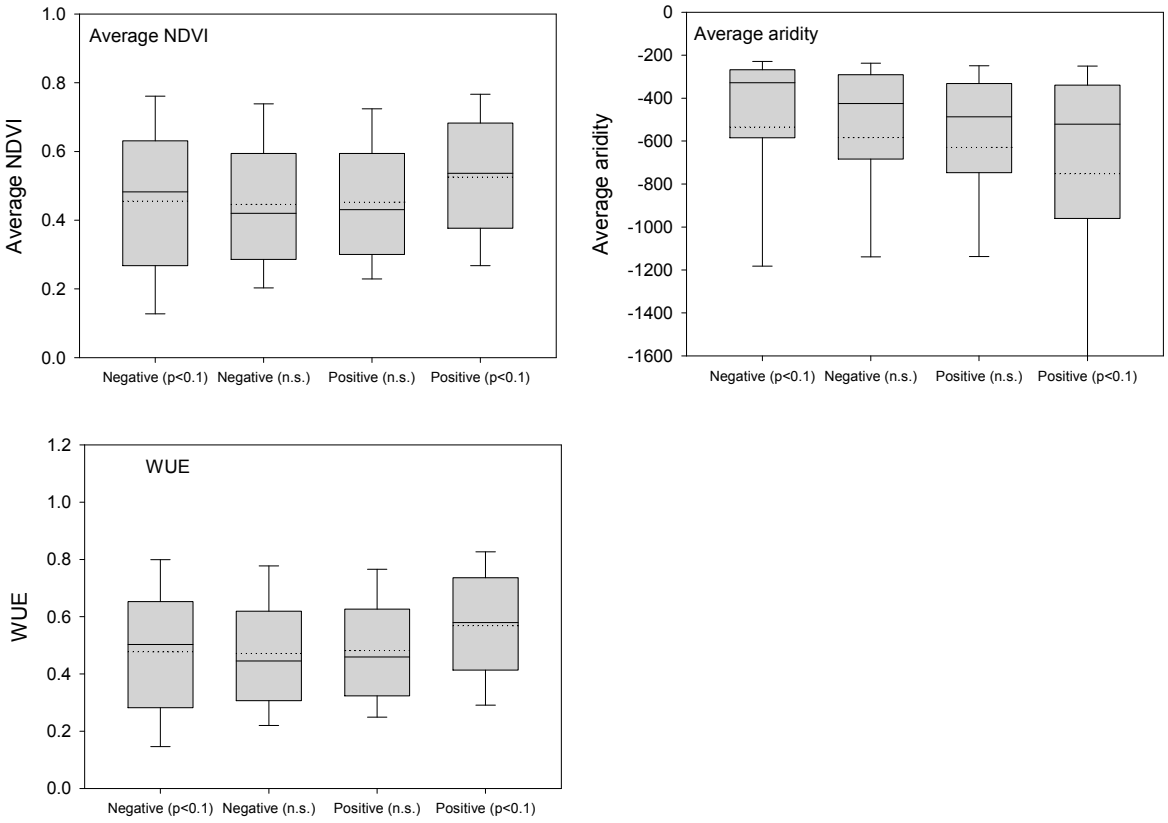

Figure 6. Box plots showing the average NDVI, aridity and Water Use Efficiency (WUE) for the four categories of NDVI trend.

3.2. Drought Influence on NDVI Variability and Trends

Figure 7 shows the spatial distribution of the Pearson's *r* correlation coefficient between the SPEI and $NDVI_{max}$ time series, corresponding to the SPEI time scale at which the maximum correlation between $NDVI_{max}$ and SPEI was reached. For the majority of the world's semiarid regions the correlation was positive and statistically significant (67.9% of the total surface, see Figure 8), which highlights the importance of water availability in explaining variability in $NDVI_{max}$ in these areas. Strong correlations were found for Australia, South Africa and Namibia, areas of the Sahel, southern USA, northern Mexico and northern Maghreb. Figure 9 shows box plots of the average maximum $NDVI_{max}$, climate aridity and WUE, corresponding to the categories of SPEI *vs.* $NDVI_{max}$ correlations. Areas showing a positive and significant correlation between $NDVI_{max}$ and the SPEI generally showed lower values of $NDVI_{max}$ than the other categories. This was also observed for the WUE. Nevertheless, the differences were not statistically significant according to the ANOVA analysis. The box plot of the climate aridity as a function of the four SPEI-$NDVI_{max}$ correlation categories shows that the areas having positive and significant correlations between $NDVI_{max}$ and the SPEI correspond to more arid areas than the regions showing negative or positive but non-significant correlations. There was a clear aridity gradient between the various categories of correlation between the SPEI and $NDVI_{max}$. The differences of aridity between the positive and negative categories were statistically significant, as well as between the positive and non-significant and the positive and significant correlations.

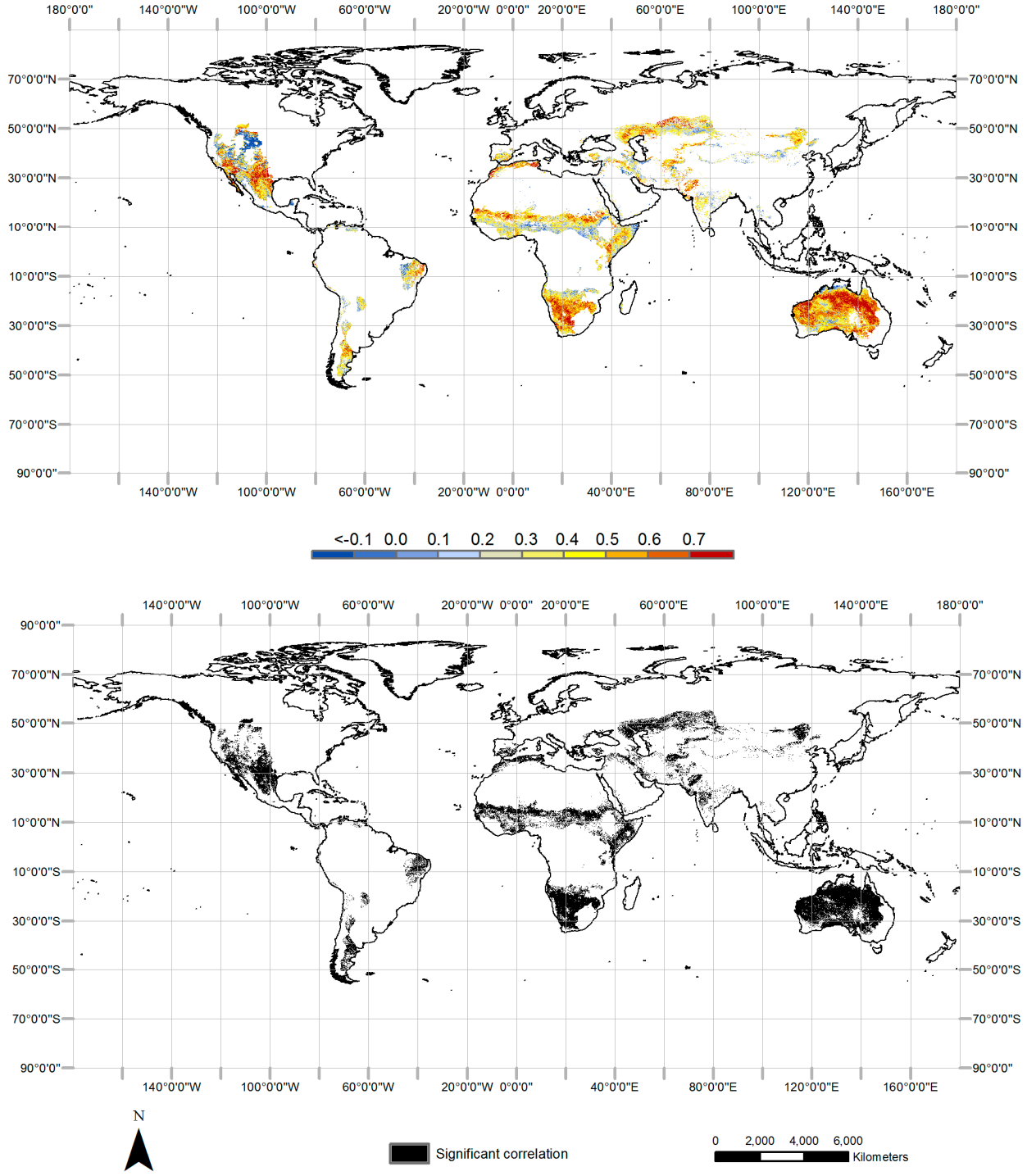

Figure 7. Pearson's r correlation coefficients between SPEI and NDVI time series in the month of maximum vegetation activity (1982–2011). Top: magnitude of Pearson's *r* correlations. Bottom: areas (in black) having positive and significant correlations between the SPEI and NDVI ($p < 0.1$).

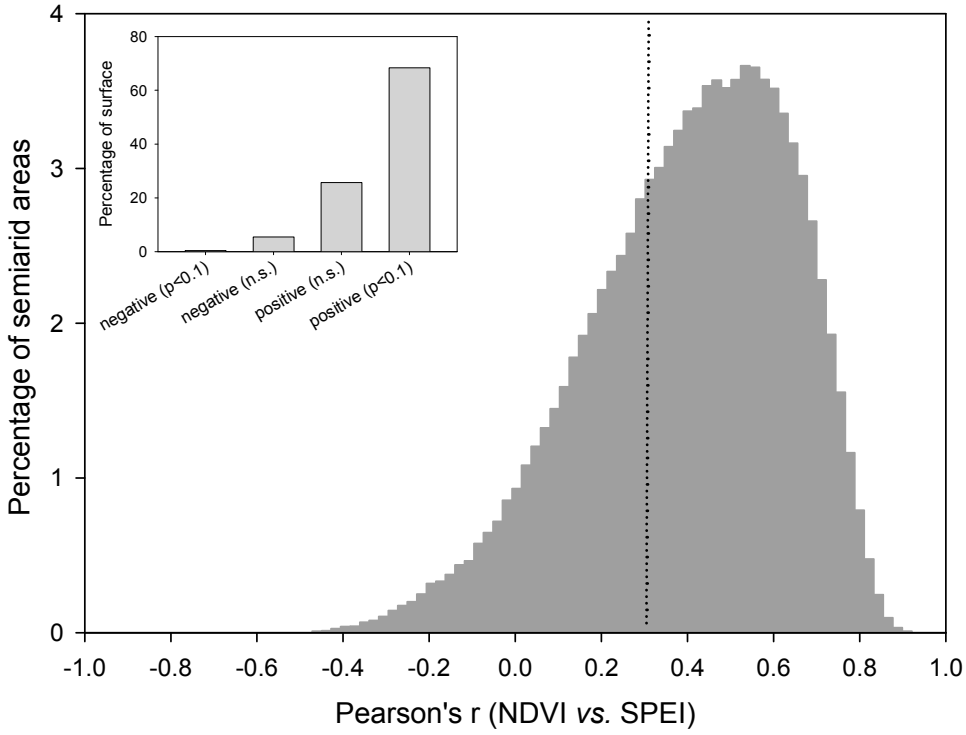

Figure 8. Percentage of semiarid regions according to the correlation coefficient between the NDVI and SPEI (1982–2011). The inset plot shows the percentages of semiarid lands having negative and positive trends (including signification).

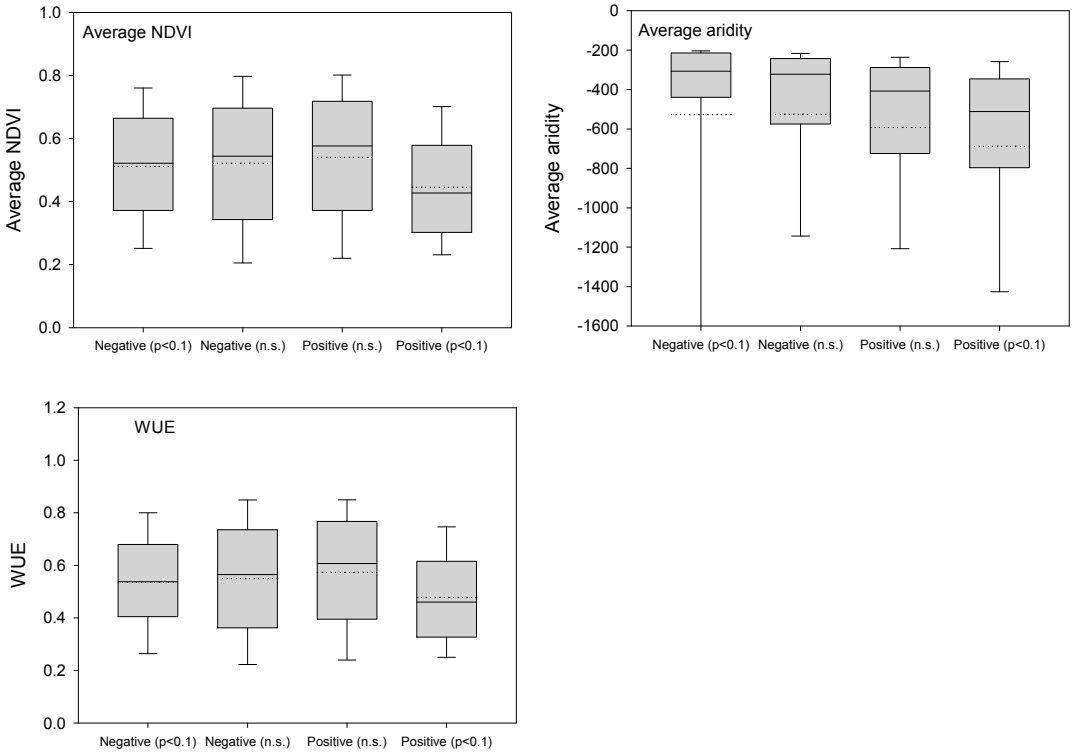

Figure 9. Box plots showing the average NDVI, aridity and WUE for the four categories of correlation between the SPEI and NDVI.

3.3. Trends in SPEI

Figure 10 shows the evolution of the SPEI corresponding to the month in which the maximum vegetation activity was identified in each pixel, and the SPEI time scale at which the maximum SPEI/NDVI$_{max}$ correlation was identified. In areas of the Sahel, Namibia and northern Australia the SPEI showed clear positive and significant trends, indicating lesser drought severity and greater water availability over the last three decades. A dominant SPEI decrease, indicative of drier conditions, was identified in North America, regions of Argentina, Asia, and inner areas of the Horn of Africa and South Australia, among others. Positive and significant SPEI trends were spatially dominant with respect to negative and significant trends at the global scale (18.9% *vs.* 8.6%, respectively).

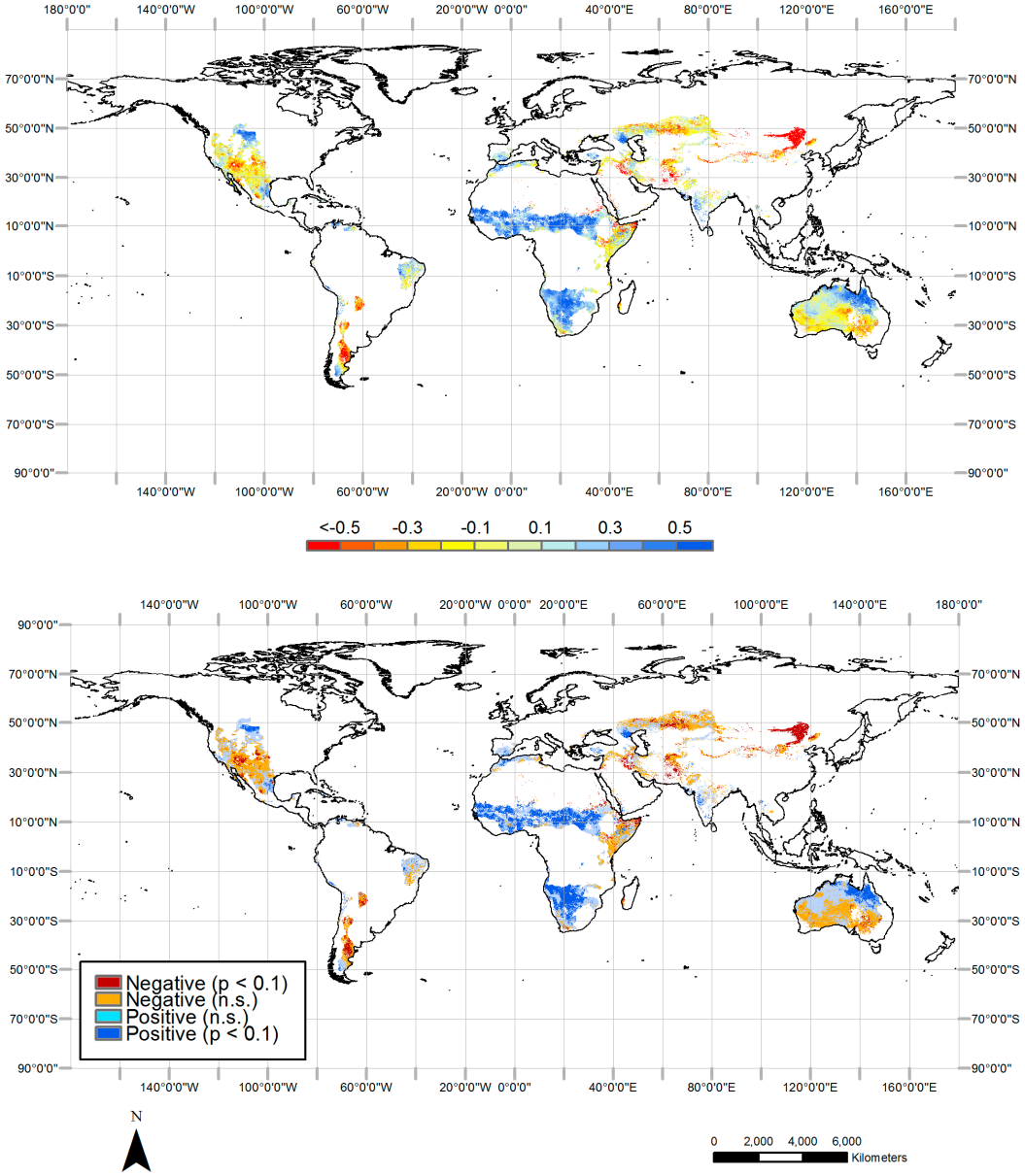

Figure 10. Trends of the SPEI (1982–2011) corresponding to the month of maximum vegetation activity and the SPEI time scale at which the maximum SPEI/NDVI correlation was identified in each pixel. (**Top**) magnitude of the trends (in SPEI units decade^{-1}). (**Bottom**) sign and signification ($p < 0.1$) of the trends.

3.4. Relationship between SPEI Trends and NDVI$_{max}$ Trends

Figure 11 provides a scatterplot showing the observed magnitude of change of NDVI$_{max}$ and the magnitude of change in the SPEI during the month of average maximum NDVI and the SPEI time-scale that recorded the highest correlation. Although not strong, the spatial relationship between both parameters was positive, indicating that positive SPEI trends tend to favor positive NDVI$_{max}$ trends. This was clearly evident in the cross-tabulation analysis. Table 1 shows that the sign and significance of the trends in the SPEI were significantly correlated to the sign and trend of NDVI$_{max}$. The Coefficient of Contingency was significant, indicating that a significant decrease of the SPEI favors a decrease in NDVI$_{max}$, and *vice versa*. Thus, the various categories of NDVI$_{max}$ trends clearly corresponded to different populations of SPEI change. Figure 12 provides a box plot showing the magnitudes of change in the SPEI corresponding to the four categories of NDVI$_{max}$ trend noted above. Clearly there is a gradient between negative NDVI$_{max}$ trends, in which the magnitude of change in the SPEI tends to be negative, and the positive NDVI$_{max}$ trends that coincide with positive magnitudes of change.

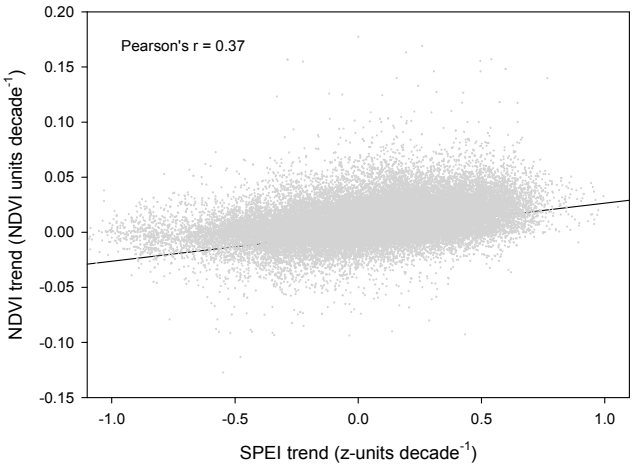

Figure 11. Relationship between the magnitude of the NDVI and SPEI trends (units decade^{-1}) between 1982 and 2011 for the world's semiarid regions.

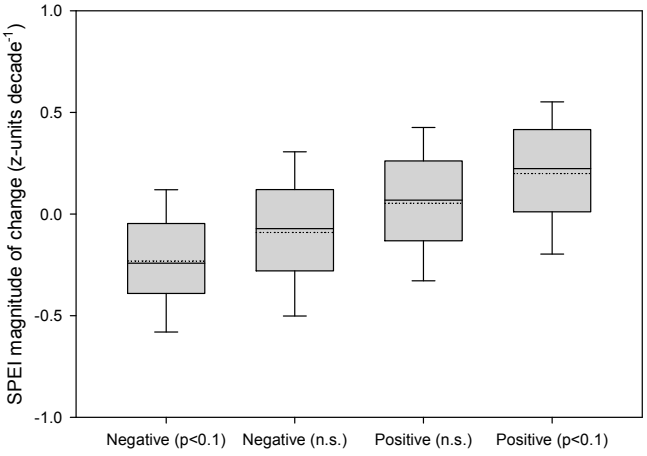

Figure 12. Box plot showing the magnitude of change in the SPEI corresponding to the categories of NDVI trend between1982 and 2011.

Table 1. Association between the sign and signification of the NDVI and the SPEI trends according to the cross-tab analysis. The chi-square and the coefficient of contingency (CC) are shown.

Chi-Square	**5293,838**
sig	<0.000
CC	**0.350**
sig	<0.000

3.5. Evolution of Residual Series

Figure 13 shows an example of the evolution of the residual series at two sites. The left upper plot shows the evolution of the April NDVI (corresponding to the month having the average maximum NDVI) and the four-month SPEI (the time scale at which the maximum correlation was found), at 91°E, 31.2°N (North America). The left middle plot shows the evolution of the observed *vs.* predicted NDVI, based on a regression model in which the four-month SPEI was the predictor. The residual (the difference between observed and predicted) is shown in the bottom plot. The plot shows a clear positive trend in the residual, indicative of a NDVI increase greater than expected by the evolution of the SPEI. In contrast, at 2.5°E, 35.5°N the opposite occurred, whereby the predicted NDVI was higher than that expected by the SPEI evolution, which suggests that factors other than water availability during the month in which the maximum NDVI was recorded may have affected the evolution of the NDVI. Figure 14 shows the spatial distribution of the sign and signification of the evolution of residuals in the regions in which a significant correlation between $NDVI_{max}$ and SPEI was observed. This shows dominant negative trends in regions of Namibia, South Africa, North America and Argentina, but dominant positive trends in the Sahel, Mexico, northeast Brazil, and central and South Australia. Thus, there was a dominant increase of residuals at the global scale, with >25% of the analyzed areas showing a positive and significant increase, and 64% showing positive coefficients (Figure 15).

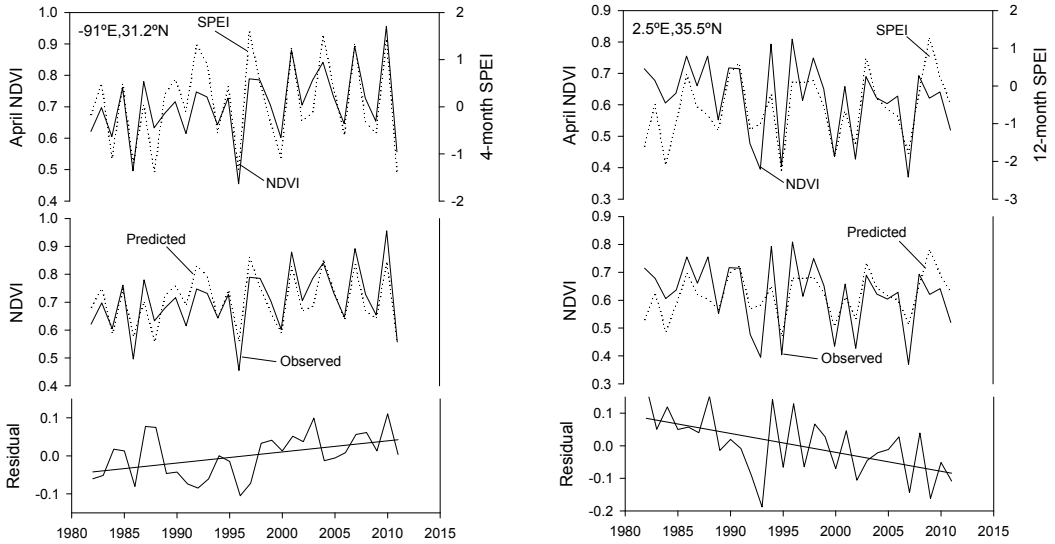

Figure 13. Examples of the evolution of residuals between NDVI observations and predictions, using the SPEI as predictor. Left: USA at −91°E, 31.2°N, Right: Algeria at 2.5°E, 35.5°N.

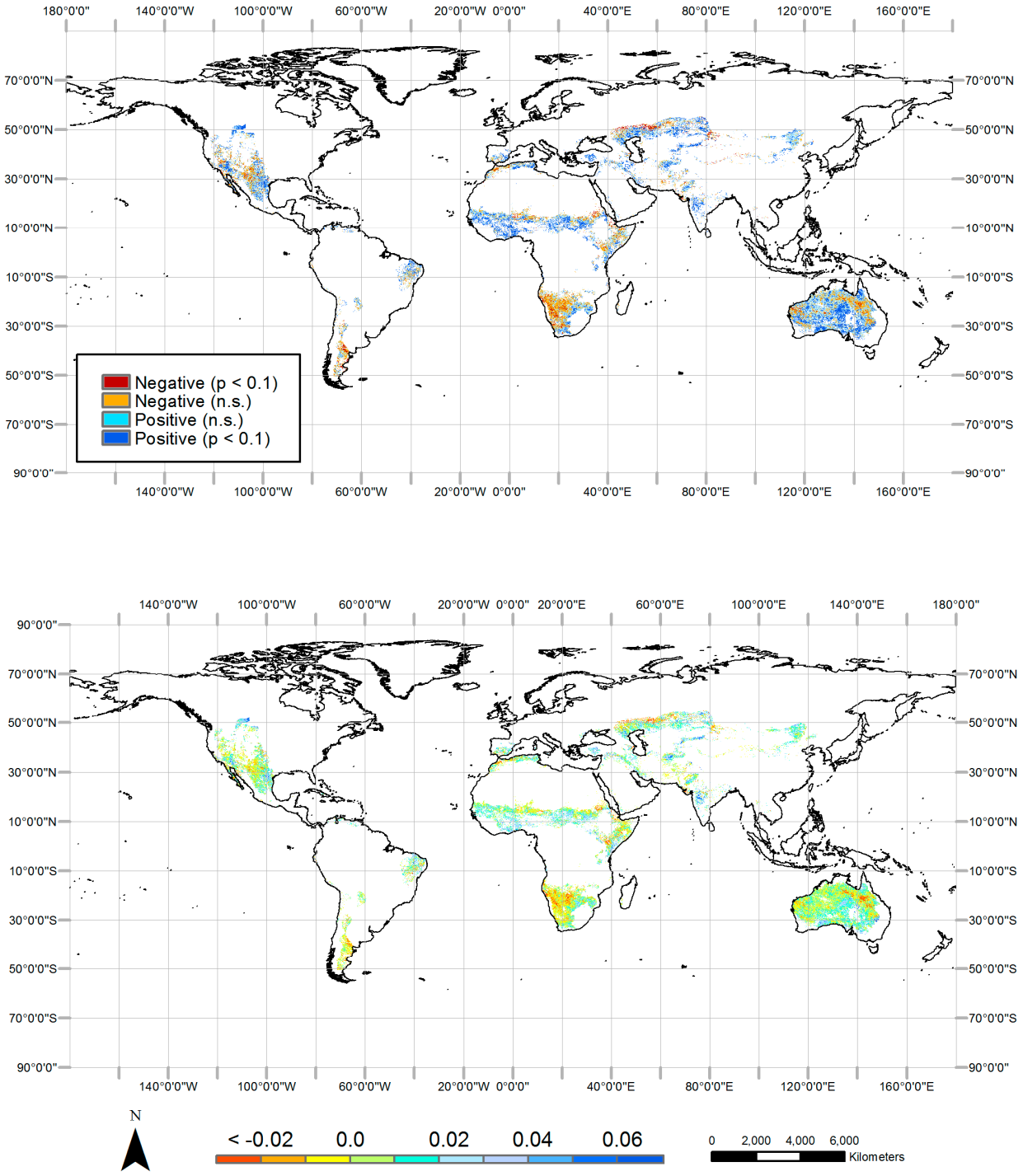

Figure 14. Trend in residual series (difference between observed and predicted NDVI, according to variations of SPEI) in areas having positive and significant correlations between the SPEI and NDVI. Top: sign and signification ($p < 0.1$) in the trend of the residual series. Bottom: magnitude of the residual series (in NDVI units decade^{-1}).

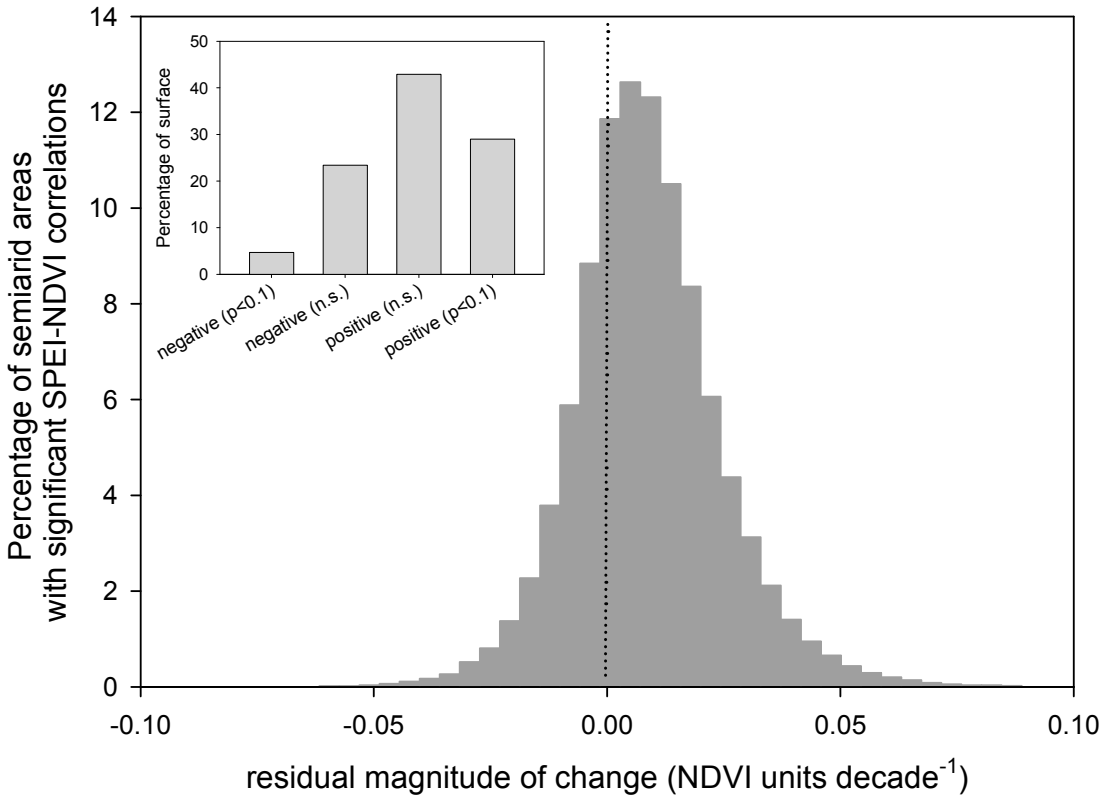

Figure 15. Percentage of semiarid regions in which there was a significant correlation between the SPEI and NDVI, according to the magnitude of change in the residual series. The inset plot shows the percentages of the analyzed lands having negative and positive trends of the residuals (including signification).

The residual trends category showed a level of control exerted by the spatial distribution over some of the factors analyzed (Figure 16). No marked differences were evident among category trends as a function of the average aridity, the WUE or the observed change in SPEI. There were no significant differences among the values of these variables as a function of the trend categories of residuals. Nevertheless, we detected patterns for the average $NDVI_{max}$ for the period 1982–2011 for each 8-km cell. Areas showing positive and significant trends for the series of residuals in general showed higher average $NDVI_{max}$ values than areas showing negative trends. The pattern was much clearer for the observed change in the $NDVI_{max}$. The areas showing positive and significant trends in the series of residuals were in general characterized by dominant positive trends in the $NDVI_{max}$ values, whereas the areas showing negative and significant trends in the series of residuals tended to show negative trends in $NDVI_{max}$ values. The differences among the groups were statistically significant.

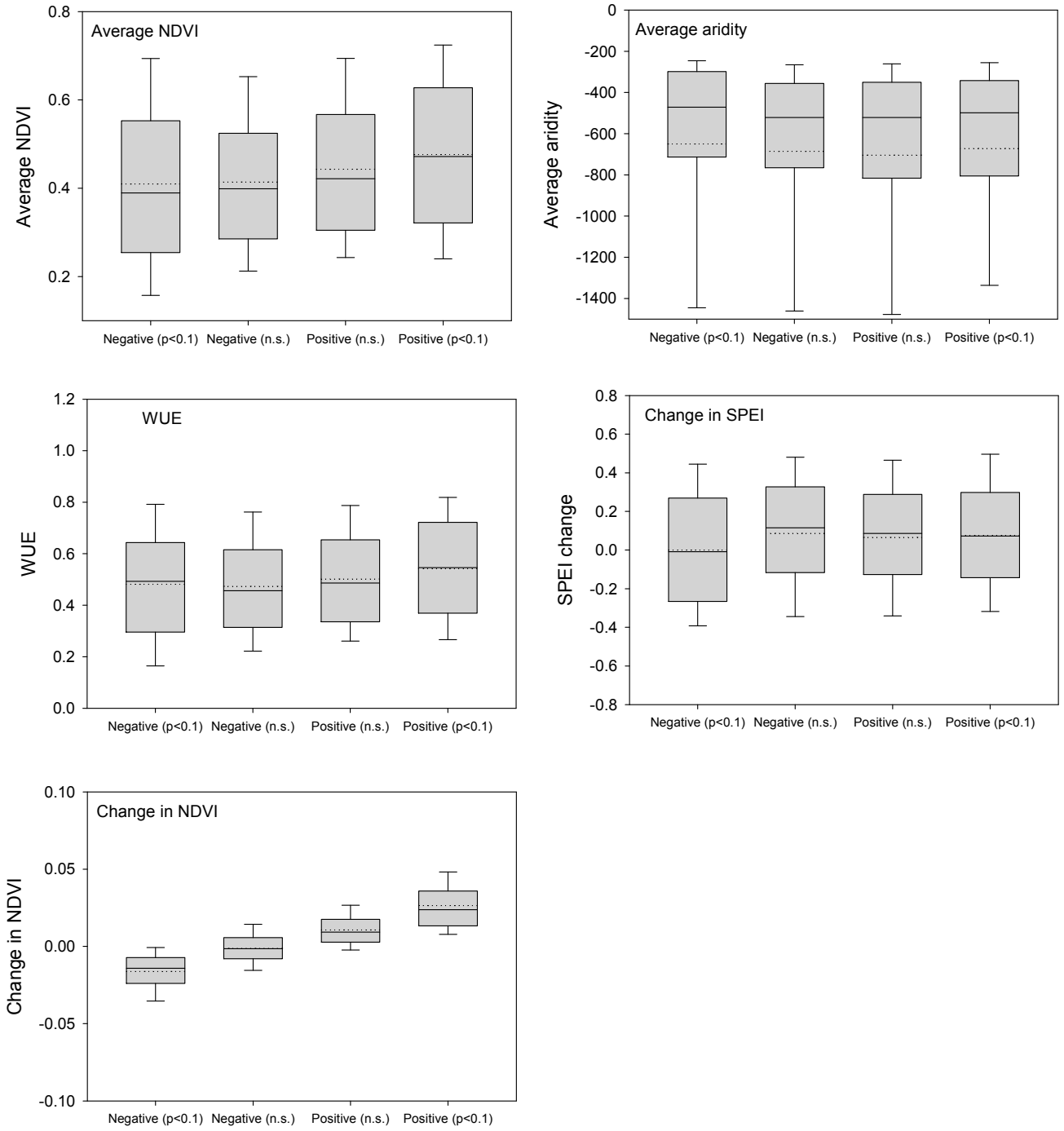

Figure 16. Box plots showing the average NDVI, aridity, WUE and magnitude of change in the SPEI and NDVI in the four categories of trend in the residual series.

4. Discussion

In this study we used the GIMMS dataset to analyze trends in the Normalized Difference Vegetation Index (NDVI) in the world's semiarid regions, based on 30 years of NOAA-AVHRR images. We investigated the influence of drought events on semiarid land degradation processes using a multi-scalar drought index (the Standardized Precipitation Evapotranspiration Index; SPEI), which took into account both precipitation and the atmospheric evaporative demand, and was able to be calculated at different time scales to take account of the varied times of response of vegetation activity to water availability.

4.1. Vegetation Activity Trends

The NDVI values recorded during the period of maximum vegetation activity ($NDVI_{max}$) showed a dominant positive evolution in the majority of the world's semiarid regions between 1982 and 2011; this was very evident for the Sahel, northeast Brazil, east Mexico, Australia, and in other smaller areas. Thus, 73% of the semiarid regions showed a positive evolution of the $NDVI_{max}$ in the month of maximum activity, although only 33% of the regions showed a positive and statistically significant trend. In contrast, 22% of the areas showed a negative trend in $NDVI_{max}$, and only 5% of these were statistically significant. These results are consistent with a number of regional and global studies on the evolution of vegetation activity in semiarid regions [15,16,34,51]. Although these were based on monthly maximum value composites of NDVI values or integrated annual values, the results are comparable with the results we found using $NDVI_{max}$.

Fensholt *et al.* [16] also used the AVHRR-GIMMS dataset for the period 1981–2007 to determine monthly trends of NDVI in the world's semiarid regions. They showed dominance of vegetation greenness in semiarid areas between 1981 and 2007, and concluded that "*current generalizations, claiming that land degradation is ongoing in semiarid areas worldwide, are not supported by the satellite based analysis of vegetation greenness*". These results are consistent with the evolution of $NDVI_{max}$ over the period 1981–2011, confirming that maximum biomass productivity in semiarid ecosystems may have increased in recent decades. This pattern could be indicative of less constraining environmental conditions as a consequence of increased soil water availability. The most representative case is probably the Sahel, where various studies have documented this pattern [15,76]. Thus, field studies in the region have indicated that flora diversification has occurred since the mid-1990s as a response to more precipitation [77]. Nevertheless, we note that regional and local variability can occur, and that greening recorded in some areas using remote sensing data does not necessarily mean that land degradation processes are absent, as an increase in vegetation cover concentrated in a few areas could produce vegetation greening but mask accompanying degradation processes. Herrman and Tappan [78] recently used long-term field surveys to show that despite greening in central Senegal, impoverishment of the vegetation cover had occurred at various study sites, as indicated by an overall reduction in species richness, an increase in the dominance of shrubs, and a shift towards more arid-tolerant species. Schlesinger *et al.* [79] and Reynolds *et al.* [80] detailed similar processes in semiarid areas of North America. They found that an increase in shrub cover and density (and greening) could be accompanied by land degradation processes, because the cycling of nutrients was progressively confined to the zones of litter accumulation beneath shrubs, while the bare inter-shrub spaces became increasingly nutrient poor, and subject to overland flow, soil erosion by wind and water, and nutrient losses. The replacement of herbaceous plants by shrubs, and the progressive development of shrub resource islands is considered to be an early warning sign of desertification [5], which could be independent of the greening trends found in some regions of the world.

We also note that land degradation processes are scale-dependent and that the spatial resolution used in this study (8 × 8 km) could mask land degradation processes only evident at a smaller scale. Stellmes *et al.* [81] compared land degradation processes using time series of Landsat (30 m) and NOAA-AVHRR images (1.1 km) in northern Greece, and showed that although the high temporal

resolution of NOAA-AVHRR enables the use of enhanced time series methods, several cover modifications can only be assessed using long-term field surveys or high resolution time series, such as provided by Landsat TM/ETM+. This is common in complex semiarid landscapes in which land degradation processes are evident at very small spatial scales [17,82,83]. The large-scale study presented here identifies the main features of vegetation changes in the world's semiarid regions, but cannot provide details of particular processes identified at regional or local scales, some of which are highly complex. These include processes observed in Mediterranean regions, in which the magnitude of the response of the vegetation to drought is very sensitive to differences among sites, seasons, and species, but also to interactions with different environmental factors that determine plant conditions [84,85], and where centuries of significant human pressure have interacted with climate change and drought to produce mosaics of land degradation processes [17,19].

4.2. Influence of the Drought Variability on Vegetation Activity

A number of previous studies have noted the marked influence of interannual precipitation variability on the NDVI [47,86–89]. We found that for the majority of world's semiarid regions the NDVI values during the peak of maximum vegetation activity were highly correlated with drought variability, evaluated using the SPEI. Several previous studies have reported that the influence of rainfall on interannual NDVI variability is not very strong, including in semiarid regions as South Africa [90] and the Sahel [73,91]. Hein *et al.* [92] reported that the response of semiarid vegetation to precipitation variability can be disturbed by other factors including nutrient status, lag effects between precipitation and subsequent vegetation activity and growth [47], and rainfall-runoff relationships, which are determined by the intensity of particular rainfall events.

In our study we showed that there was a positive and significant correlation between the SPEI and NDVI in 68% of the area of semiarid regions of the world. The SPEI is probably more suited to identifying the influence of water availability and drought severity on the vegetation dynamics in semiarid regions than is precipitation, as the SPEI is based on the combined climatic water balance (precipitation minus AED), and takes into account the strong atmospheric evaporative demand that is typical of semiarid regions. Recent studies using tree-ring records have shown that in various regions under current global warming conditions the AED can have a greater influence on the vegetation dynamics than does precipitation [93–95], as AED largely determines the soil and plant water stress. Thus, Stephenson [96] showed that the evapotranspiration deficit is a better metric than precipitation for explaining the current distribution of vegetation communities at the global scale. Moreover, the SPEI is computed on different time scales, enabling identification of the most suitable time scale to detect the varied response times of vegetation communities to water deficits [30,97]. This approach is undoubtedly preferable to identifying drought impacts on vegetation activity and growth based on annual precipitation, and has usually been used in studies analyzing the influence of climate on the NDVI in semiarid regions [98–100].

We found that the trends in drought events exerted an influence on the $NDVI_{max}$ trends at the global scale. The relationship between the trends in these variables was not strong, but at a spatial level was statistically significant. Thus, the semiarid regions that showed a greater increase in $NDVI_{max}$ (the Sahel, northern Australia, South Africa) were characterized by a clear positive trend in the SPEI

values, indicative of more humidity and lesser drought conditions. Thus, the categories of $NDVI_{max}$ trends clearly showed significant differences in the magnitude of change in the SPEI (positive changes for positive $NDVI_{max}$ trends, and negative changes for negative $NDVI_{max}$ trends).

4.3. Other Possible Explanatory Factors

A number of studies have considered the important role of droughts in triggering land degradation processes [6,12,13]. Nevertheless, although changes in drought severity may be an important driver of NDVI trends and land degradation processes in semiarid regions, it is important to note that the results obtained in the present study suggest that drought may not explain several of the observed changes in $NDVI_{max}$. The residuals of the models created to predict the $NDVI_{max}$ evolution based on the SPEI showed that the trend in residuals was predominantly positive throughout semiarid regions, and that the observed spatial patterns were not related to the average NDVI, climate aridity or WUE conditions. Thus, positive trends in the residuals of the models were mainly found to occur in areas characterized by large increases in the NDVI, including the Sahel, central Australia, southern and northern America and northeast Brazil. The observed trends and the response of droughts in various semiarid regions of the world suggest marked resilience of semiarid ecosystems; although some studies have suggested drought as the primary driver of land degradation in areas of Africa [12,73], these areas showed an increase in potential production that was much greater than expected by the evolution of drought severity.

Le Houerou [6] reported that under conditions of sufficient soil water content a CO_2-enriched atmosphere could enhance photosynthesis, plant size and overall productivity, and reduce stomatal conductance and transpiration in semiarid ecosystems, thus improving the WUE. Fensholt *et al.* [16] and Donohue *et al.* [101] suggested atmospheric CO_2 fertilization [102] as the most plausible explanation for the generalized greening observed in the world's semiarid regions, in excess of the estimated climate potential. Nevertheless, the effects of CO_2 fertilization are not uniform [103], and are determined by the availability of water and other nutrients. Thus, Smith *et al.* [104] showed that CO_2 fertilization would not enhance production under drought conditions because, independent of the atmospheric CO_2 concentration, plant physiological processes are highly constrained by water deficits, and also by nitrogen limitations [105]. This could help explain why we found a general negative trend of $NDVI_{max}$ in the regions characterized by negative SPEI trends (e.g., Argentina, southern USA and areas of the Horn of Africa), as water deficits could limit the influence of CO_2 fertilization in these regions.

In addition to drought evolution and CO_2 fertilization, other local to regional factors should be analyzed to understand current NDVI trends in semiarid regions. Factors including the abandonment of traditional land uses (with consequent increase of shrub cover potentially increasing the risk of severe forest fires), increased grazing or cropping, and the loss of soil fertility through salinization or decreased organic content (with consequent loss of moisture retention) could explain the NDVI decrease in some areas, and land cover changes and human land intensification could explain the increased greening observed in some regions. Olsson *et al.* [15] concluded that climate trends cannot fully explain the changes in vegetation activity in the Sahel, and that other factors including land use changes and migration may contribute. Evans and Geerken [31] showed that the expansion of

agriculture was responsible for the positive NDVI trends observed in the drylands of Syria. Begué *et al.* [106] suggested that the increase of the NDVI in the Sahel region may be the consequence of high cropping rates. Thus, Brink and Eva [107] reported an increase of 14% and 26% in the cropland classes for the period 1975–2000 in the Sahel and Sudan ecoregions, respectively. In addition, increased investment and improvements in soil and water conservation techniques, such as contour bunding, in response to drought crises experienced by farmers could explain positive trends [108]. The importance of human factors, including decisions on production strategies and land use, in contributing to environmental and vegetation change over long time periods must also be taken into account [109]. Some studies have noted that higher stocking rates may favor vegetation recovery because herbivores reduce the aboveground grass biomass, but they lead to a reduction of fine fuel and a consequent reduction or complete elimination of grassland fires [110].

We showed that areas having dominant negative trends in residuals, including Namibia, Argentina and regions of southern USA, Somalia, Ethiopia and Australia showed a general negative trend in the $NDVI_{max}$. In these areas the $NDVI_{max}$ has decreased to a greater extent than expected with the evolution of drought conditions. These areas show a strong correlation between the NDVI and the SPEI, but the mechanisms that have caused a greater decrease of the $NDVI_{max}$ than that expected from the SPEI evolution may be driven by various factors. In southern USA and Argentina the SPEI trends have been predominantly negative. This could mean that lower water availability reinforces the effect of other driving factors (e.g., grazing). In other areas including Namibia and regions of Australia the SPEI trends have been positive, but under these more favorable conditions the $NDVI_{max}$ has not significantly increased, which suggests that other factors (e.g., human, edaphic, ecological) could be influential.

5. Conclusions

In this study we used the the Global Inventory Monitoring and Mapping Studies (GIMMS) dataset to analyze trends in the Normalized Difference Vegetation Index (NDVI) in the world's semiarid regions, based on 30 years of National Oceanic and Atmospheric Administration-Advanced Very High Resolution Radiometer (NOAA-AVHRR) images. We investigated the influence of drought events on semiarid land degradation processes using a multi-scalar drought index (the Standardized Precipitation Evapotranspiration Index; SPEI), which took into account both precipitation and the atmospheric evaporative demand, and was able to be calculated at different time scales to take account of the varied times of response of vegetation activity to water availability. The main conclusions of this study are:

i. Positive trends in $NDVI_{max}$ clearly dominated across the world's semiarid regions for the period 1982–2011.
ii. Areas showing negative and significant trends in $NDVI_{max}$ mostly corresponded to areas associated with lower climate aridity, whereas the areas showing positive and significant NDVImax trends in general corresponded to the most arid regions.
iii. For the majority of the world's semiarid regions the correlation between drought and the maximum annual $NDVI_{max}$ was positive and statistically significant.

iv. There is a gradient between negative $NDVI_{max}$ trends, in which the magnitude of change in drought severity tends to be negative, and the positive $NDVI_{max}$ trends that coincide with changes toward less drought severity.
v. Non-predicted $NDVI_{max}$ evolution based on drought severity showed predominantly positive residuals throughout semiarid regions, which means an increase in potential production much greater than expected by the evolution of drought severity, but several local and regional differences have been found.

These conclusions all highlight the complexity of vegetation activity processes in the world's semiarid regions, and the difficulty of defining a universal response to the effect of drought, as a variety of factors (natural and anthropogenic) interact in these regions. Further studies, from local to regional scales, are needed to understand the variety of ways in which current drought variability, frequency and severity is affecting land degradation and land recovery in the world's semiarid lands. This is essential considering the current drought projections under global climate models for the end of 21st century, which indicate that droughts will increase [11], mostly as a consequence of warmer conditions and enhanced Atmospheric Evaporative Demand (AED) [10].

Acknowledgments

The authors thank the NASA Global Inventory Modeling and Mapping Studies (GIMMS) group for producing and sharing the AVHRR GIMMS NDVI dataset. We would also like to thank the Climate Research Unit of the University of East Anglia (UK) for providing climate data. This work was supported by the research projects CGL2011-27574-CO2-02, CGL2011-24185, CGL2014-52135-C03-01 and *Red de variabilidad y cambio climático* RECLIM (CGL2014-517221-REDT) financed by the Spanish Commission of Science and Technology and FEDER and "LIFE12 ENV/ES/000536-Demonstration and validation of innovative methodology for regional climate change adaptation in the Mediterranean area (LIFE MEDACC)" financed by the LIFE programme of the European Commission. Cesar Azorin-Molina was supported by the JCI-2011-10263 grant. Miquel Tomas-Burguera was supported by a doctoral grant by the Ministry of Economy and Competitiveness and Natalia Martin-Hernandez was supported by a doctoral grant by the Aragón Regional Government.

Author Contributions

Sergio M. Vicente-Serrano had the original idea for the study and, with all co-authors carried out the design. Sergio M. Vicente-Serrano were responsible for recruitment and follow-up of study participants. Sergio M. Vicente-Serrano, Daniel Cabello and Natalia Martín-Hernández were responsible for data cleaning and Sergio M. Vicente-Serrano, Miquel Tomás-Burguera and Santiago Beguería carried out the analyses. Sergio M. Vicente-Serrano, Daniel Cabello, Cesar Azorin-Molina and Ahmed El Kenawy drafted the manuscript, which was revised by all authors. All authors read and approved the final manuscript.

Conflicts of Interest

The authors declare no conflict of interest.

References

1. Chaves, M.M.; Maroco, J.P.; Pereira, J.S. Understanding plant responses to drought—From genes to the whole plant. *Funct. Plant. Biol.* **2003**, *30*, 239–264.
2. Le Houérou, H.N. Rain use efficiency: A unifying concept in arid-land ecology. *J. Arid Environ.* **1984**, *7*, 213–247.
3. Dregne, H.E. Land degradation in the drylands. *Arid Land Res. Manag.* **2002**, *16*, 99–132.
4. D'Odorico, P.; Bhattachan, A.; Davis, K.F.; Ravi, S.; Runyan, C.W. Global desertification: Drivers and feedbacks. *Adv. Water Resour.* **2013**, *51*, 326–344.
5. Kéfi, S.; Rietkerk, M.; Alados, C.L.; Pueyo, Y.; Papanastasis, V.P.; ElAich, A.; de Ruiter, P.C. Spatial vegetation patterns and imminent desertification in Mediterranean arid ecosystems. *Nature* **2007**, *449*, 213–217.
6. Le Houérou, H.N. Climate change, drought and desertification. *J. Arid Environ.* **1996**, *34*, 133–185.
7. Puigdefábregas, J.; Mendizabal, T. Perspectives on desertification: Western Mediterranean. *J. Arid Environ.* **1998**, *39*, 209–224.
8. Barnosky, A.D.; Hadly, E.A.; Bascompte, J.; Berlow, E.L.; Brown, J.H.; Fortelius, M.; Getz, W.M.; Harte, J.; Hastings, A.; Marquet, P.A.; *et al.* Approaching a state shift in Earth's biosphere. *Nature* **2012**, *486*, 52–58.
9. Trenberth, K.E. Changes in precipitation with climate change. *Climate Res.* **2011**, *47*, 123–138.
10. Sherwood, S.; Fu, Q. A drier future? *Science* **2014**, *343*, doi: 10.1126/science.1247620.
11. Dai, A. Drought under global warming: A review. *Wiley Interdiscip. Rev. Clim. Change* **2011**, *2*, 45–65.
12. Nicholson, S.E.; Tucker, C.J.; Ba, M.B. Desertification, drought and surface vegetation: An example from the west African Sahel. *Bull. Am. Meteorol. Soc.* **1998**, *79*, 815–829.
13. Pickup, G. Desertification and climate change—The Australian perspective. *Climate Res.* **1998**, *11*, 51–63.
14. Hickler, T.; Eklundh, L.; Seaquist, J.W.; Smith, B.; Ardö, J.; Olsson, L; Sykes, M.T.; Sjöström, M. Precipitation controls Sahel greening trend. *Geophys*. *Res. Lett.* **2005**, *32*, doi:10.1029/2005GL024370.
15. Olsson, L.; Eklundh, L.; Ardo, J. A recent greening of the Sahel—Trends, patterns and potential causes. *J. Arid Environ.* **2005**, *63*, 556–566.
16. Fensholt, R.; Langanke, T.; Rasmussen, K.; Reenberg, A.; Prince,S.D.; Tucker, C.; Scholes, R.J.; Le, Q.B.; Bondeau, A.; Eastman, R.; *et al.* Greenness in semi-arid areas across the globe 1981–2007—An earth observing satellite based analysis of trends and drivers. *Remote Sens. Environ.* **2012**, *121*, 144–158.
17. Vicente-Serrano, S.M.; Zouber, A.; Lasanta, T.; Pueyo, Y. Dryness is accelerating degradation of vulnerable shrublands in semiarid Mediterranean environments. *Ecol. Monogr.* **2012**, *82*, 407–428.
18. Le Houérou, H.N. Man-made deserts: Desertization processes and threats. *Arid Land Res. Manag.* **2002**, *16*, 1–36.

19. Alados, C.L.; Puigdefábregas, J.; Martínez-Fernández, J. Ecological and socio-economical thresholds of land and plant-community degradation in semi-arid Mediterranean areas of southeastern Spain. *J. Arid Environ.* **2011**, *75*, 1368–1376.
20. Pueyo, Y.; Alados, C.L.; García-Ávila, B.; Kéfi, S.; Maestro, M.; Rietkerk, M. Comparing direct abiotic amelioration and facilitation as tools for restoration of semiarid grasslands. *Restor. Ecol.* **2009**, *17*, 908–916.
21. Narasimha-Rao, R.V.; Venkataratuam, L.; Krishna, P.V.; Ramana, K.V. Relation between root zone soil moisture and normalized difference vegetation index of vegetated fields. *Int. J. Remote Sens.* **1993**, *14*, 441–449.
22. Davenport, M.L.; Nicholson, S.E. On the relation between rainfall and the normalized difference vegetation index for diverse vegetation types in east Africa. *Int. J. Remote Sens.* **1993**, *14*, 2369–2389.
23. Xu, J.; Ren, L.-L.; Ruan, X.-H.; Liu, X.-F.; Yuan, F. Development of a physically based PDSI and its application for assessing the vegetation response to drought in northern China. *J. Geophys. Res.: Atmos.* **2012**, *117*, doi:10.1029/2011JD016807.
24. Li, F.; Zhao, W.; Liu, H. The response of aboveground net primary productivity of desert vegetation to rainfall pulse in the temperate desert region of Northwest China. *PLoS One* **2013**, *8*, doi:10.1371/journal.pone.0073003.
25. Gutman, G. Towards monitoring droughts from space. *J. Climate* **1990**, *3*, 282–295.
26. Walsh, S.J. Comparison of NOAA-AVHRR data to meteorological drought indices. *Photogramm. Eng. Remote Sens.* **1987**, *53*, 1069–1074.
27. Lotsch, A.; Friedl, M.A.; Anderson, B.T. Coupled vegetation-precipitation variability observed from satellite and climate records. *Geophys. Res. Lett.* **2003**, *30*, doi:10.1029/2003GL017506.
28. Quiring, S.M.; Ganesh, S. Evaluating the utility of the Vegetation Condition Index (VCI) for monitoring meteorological drought in Texas. *Agric. For. Meteorol.* **2010**, *150*, 330–339.
29. Vicente-Serrano, S.M. Evaluating the impact of drought using remote sensing in a Mediterranean, semi-arid region. *Nat. Hazards* **2007**, *40*, 173–208.
30. Vicente-Serrano, S.M.; Gouveia, C.; Camarero, J.J.; Beguería, S.; Trigo, R.; López-Moreno, J.I.; Azorín-Molina, C.; Pasho, E.; Lorenzo-Lacruz, J.; Revuelto, J.; *et al*. The response of vegetation to drought time-scales across global land biomes. *Proc. Natl. Acad. Sci. USA* **2013**, *110*, 52–57.
31. Evans, J.; Geerken, R. Discrimination between climate and human-induced dryland degradation. *J. Arid Environ.* **2004**, *57*, 535–554.
32. Wessels, K.J.; Prince, S.D.; Malherbe, J.; Small, J.; Frost, P.E.; VanZyl, D. Can human-induced land degradation be distinguished from the effects of rainfall variability? A case study in South Africa. *J. Arid Environ.* **2007**, *68*, 271–297.
33. McDowell, N.; Pockman, W.T.; Allen, C.D.; Breshears, D.D.; Cobb, N.; Kolb, T.; Plaut, J.; Sperry, J.; West, A.; Williams, D.G.; *et al*. Mechanisms of plant survival and mortality during drought: Why do some plants survive while others succumb to drought? *New Phytol.* **2008**, *178*, 719–739.
34. De Jong, R.; de Bruin, S.; de Wit, A.; Schaepman, M.E.; Dent, D.E. Analysis of monotonic greening and browning trends from global NDVI time-series. *Remote Sens. Environ.* **2011**, *115*, 692–702.

35. Bai, Z.G.; Dent, D.L.; Olsson, L.; Schaepman, M.E. Proxy global assessment of land degradation. *Soil Use Manag.* **2008**, *24*, 223–234.
36. Verón, S.R.; Paruelo, J.M.; Oesterheld, M. Assessing desertification. *J. Arid Environ.* **2006**, *66*, 751–763.
37. Vicente-Serrano, S.M.; Beguería, S.; Lorenzo-Lacruz, J.; Camarero, J.J.; López-Moreno, J.I.; Azorin-Molina, C.; Revuelto, J.; Morán-Tejeda, E.; Sanchez-Lorenzo, A. Performance of drought índices for ecological, agricultural and hydrological applications. *Earth Interact.* **2012**, *16*, 1–27.
38. Vicente-Serrano S.M.; Beguería, S.; López-Moreno, J.I. A Multi-scalar drought index sensitive to global warming: The Standardized Precipitation Evapotranspiration Index—SPEI. *J. Climate* **2010**, *23*, 1696–1718.
39. Rouse, J.W.; Hass, R.H.; Schell, J.A.; Deering, D.W.; Harlan, J.C. *Monitoring the Vernal Advancement and Retrogradation (Greenwave Effect) of Natural Vegetation*; NASA/GSFC type III Final Report; GSFC: Greenbelt, MD, USA, 1974.
40. Myneni, R.B.; Keeling, C.D.; Tucker, C.J.; Asrar, G.; Nemani, R.R. Increased plant growth in the northern high latitudes from 1981 to 1991. *Nature* **1997**, *386*, 698–702.
41. Nemani, R.R; Keeling, C.D.; Hashimoto, H.; Jolly, W.M.; Piper, S.C.; Tucker, C.J.; Myneni, R.B.; Running, S.W.Climate-driven increases in global terrestrial net primary production from 1982 to 1999. *Science* **2003**, *300*, 1560–1563.
42. Zhou, L.; Tucker, C.J.; Kaufmann, R.K.; Slayback, D.; Shabanov, N.V.; Myneni, R.B. Variations in northern vegetation activity inferred from satellite data of vegetation index during 1981 to 1999. *J. Geophys. Res.: Atmos.* **2001**, *106*, 20069–20083.
43. Beck, H.E.; McVicar, T.R.; van Dijkb, A.I.J.M.; Schellekensc, J.; de Jeua, R.A.M.; Bruijnzeela, L.A. Global evaluation of four AVHRR NDVI data sets: Intercomparison and assessment against Landsat imagery. *Remote Sens. Environ.* **2011**, *115*, 2547–2563.
44. Tucker, C.J.; Pinzon, J.E.; Brown, M.E.; Slayback, D.A.; Pak, E.W.; Mahoney, R.; Vermote, E.F.; El Saleous, N. An extended AVHRR 8-km NDVI dataset compatible with MODIS and SPOT vegetation NDVI data. *Int. J. Remote Sens.* **2005**, *26*, 4485–4498.
45. Pinzon, J.E.; Tucker, C.J. A non-stationary 1981–2012 AVHRR NDVI3g time series. *Remote Sens.* **2014**, *6*, 6929–6960.
46. Campo-Bescós, M.A.; Muñoz-Carpena, R.; Southworth, J.; Zhu, L.; Waylen, P.R.; Bunting, E. Combined spatial and temporal effects of environmental controls on long-term monthly NDVI in the Southern Africa Savanna. *Remote Sens.* **2013**, *5*, 6513–6538.
47. Zeng, F-W.; Collatz, G.J.; Pinzon, J.E.; Ivanoff, A. Evaluating and quantifying the climate-driven interannual variability in Global Inventory Modeling and Mapping Studies (GIMMS) Normalized Difference Vegetation Index (NDVI3g) at global scales. *Remote Sens.* **2013**, *5*, 3918–3950.
48. Anyamba, A.; Small, J.L.; Tucker, C.J.; Pak, E.W. Thirty-two years of Sahelian zone growing season non-stationary NDVI3g patterns and trends. *Remote Sens.* **2014**, *6*, 3101–312
49. De Jong, R.; Verbesselt, J.; Zeileis, A.; Schaepman, M.E. Shifts in global vegetation activity trends. *Remote Sens.* **2013**, *5*, 1117–1133.

50. Mao, J.; Shi, X.; Thornton, P.E.; Hoffman, F.M.; Zhu, Z.; Myneni, R.B.; Global latitudinal-asymmetric vegetation growth trends and their driving mechanisms: 1982–2009. *Remote Sens.* **2013**, *5*, 1484–1497.
51. Cook, B.I.; Pau, S. A global assessment of long-term greening and browning trends in pasture lands using the GIMMS LAI3g dataset. *Remote Sens.* **2013**, *5*, 2492–2512.
52. Bi, J.; Xu, L.; Samanta, A.; Zhu, Z.; Myneni, R. Divergent arctic-boreal vegetation changes between north America and Eurasia over the past 30 years. *Remote Sens*. **2013**, *5*, 2093–2112.
53. Dardel, C.; Kergoat, L.; Hiernaux, P.; Grippa, M.; Mougin, E.; Ciais, P.; Nguyen, C.-C. Rain-use-efficiency: What it tells us about the conflicting Sahel greening and Sahelian paradox. *Remote Sens.* **2014**, *6*, 3446–3474.
54. Fensholt, R.; Rasmussen, K.; Kaspersen, P.; Huber, S.; Horion, S.; Swinnen, E. Assessing land degradation/recovery in the African Sahel from long-term earth observation based primary productivity and precipitation relationships. *Remote Sens.* **2013**, *5*, 664–686.
55. Beguería, S.; Vicente-Serrano, S.M.; Angulo, M. A multi-scalar global drought data set: The SPEIbase: A new gridded product for the analysis of drought variability and impacts. *Bull. Am. Meteorol. Soc.* **2010**, *91*, 1351–1354.
56. Vicente-Serrano, S.M.; Beguería, S.; López-Moreno, J.I.; Angulo, M.; El Kenawy, A. A new global 0.5° gridded dataset (1901–2006) of a multiscalar drought index: comparison with current drought index datasets based on the Palmer Drought Severity Index. *J. Hydrometeorol.* **2010**, *11*, 1033–1043.
57. Vicente-Serrano, S.M.; Van der Schrier, G.; Beguería, S.; Azorin-Molina, C.; Lopez-Moreno, J.I. Contribution of precipitation and reference evapotranspiration to drought indices under different climates. *J. Hydrol*. **2014**, doi:10.1016/j.jhydrol.2014.11.025 (In press).
58. Harris, I.; Jones, P.D.; Osborn, T.J.; Lister, D.H. Updated high-resolution grids of monthly climatic observations—The CRU TS3.10 dataset. *Int. J. Climatol.* **2014**, *34*, 623–642.
59. Köppen, W. Das geographische system der klimate. In *Handbuch der Klimatologie*; Köppen, C.W., Geiger, R., Eds.; Gebrüder Bornträger: Berlin, Germany, 1936; vol. 3.
60. Budyko, M.I. *Climate and Life*; Academic: New York, NY, USA, 1974.
61. UNEP. *World Atlas of Desertification*; Edward Arnold: London, UK, 1992.
62. Holdridge, L.R. Determination of world plant formations from simple climatic data. *Science* **1947**, *105*, 367–368.
63. Kassas, M. Desertification: A general review. *J. Arid Environ.* **1995**, *30*, 115–128.
64. Tucker, C.J.; Vanpraet, C.; Boerwinkel, E.; Gaston, A. Satellite remote-sensing of total dry-matter production in the Senegalese Sahel. *Remote Sens. Environ.* **1983**, *13*, 461–474.
65. Nicholson, S.E.; Farrar, T. The influence of soil type on the relationships between NDVI, rainfall and soil moisture in semi-arid Botswana: Part I. NDVI response to rainfall. *Remote Sens. Environ.* **1994**, *50*, 107–120.
66. Fensholt, R.; Sandholt, I.; Rasmussen, M.S.; Stisen, S.; Diouf, A. Evaluation of satellite based primary production modelling in the semi-arid Sahel. *Remote Sens. Environ.* **2006**, *105*, 173–188.
67. Lanzante, J.R. Resistant, robust and non-parametric techniques for the analysis of climate data: Theory and examples including applications to historical radiosonde station data. *Int. J. Climatol.* **1996**, *16*, 1197–1226.

68. De Luis, M.; Vicente-Serrano, S.M.; González-Hidalgo, J.C.; Raventós J. Aplicación de las Tablas de Contingencia (Cross Tab análisis) al análisis espacial de tendencias climáticas. *Cuadernos. Investigación. Geográfica.* **2003**, *29*, 23–34.
69. Clark, W.A.V.; Hosking, P.L. *Statistical Methods for Geographers*; Jhon Willey & Sons: New York, NY, USA, 1986; p. 528.
70. Herrmann, S.A.; Anyamba, A.; Tucker, C.J. Recent trends in vegetation dynamics in the African Sahel and their relationship to climate. *Glob. Environ. Change* **2005**, *15*, 394–404.
71. Fensholt, R.; Rasmussen, K. Analysis of trends in the Sahelian 'rain-use efficiency' using GIMMS NDVI, RFE and GPCP rainfall data. *Remote Sens. Environ.* **2011**, *115*, 438–451.
72. Li, A.; Wu, J.; Huang, J. Distinguishing between human-induced and climate-driven vegetation changes: A critical application of RESTREND in Inner Mongolia. *Landsc. Ecol.* **2012**, *27*, 969–982.
73. Prince, S.D.; De Colstoun, E.B.; Kravitz, L.L. Evidence from rain-use efficiencies does not indicate extensive Sahelian desertification. *Glob. Change Biol.* **1998**, *4*, 359–374.
74. Paruelo, J.M.; Lauenroth,W.K.; Burke, I.C.; Sala, E.O. Grassland precipitation-use efficiency varies across a resource gradient. *Ecosystems* **1999**, *2*, 64–68.
75. Illius, A.W.; O'Connor, T.G. On the relevance of nonequilibrium concepts to arid and semiarid grazing systems. *Ecol. Appl.* **1999**, *9*, 798–813.
76. Anyamba, A.; Tucker, C.J. Analysis of Sahelian vegetation dynamics using NOAA-AVHRR NDVI data from 1981–2003. *J. Arid Environ.* **2005**, *63*, 596–614.
77. Hiernaux, P.; Diarrab, L.; Trichonc, V.; Mougin, E.; Soumagueld, N.; Baupa, F. Woody plant population dynamics in response to climate changes from 1984 to 2006 in Sahel (Gourma, Mali). *J. Hydrol.* **2009**, *375*, 103–113.
78. Herrmann, S.M.; Tappan, G.G.; Vegetation impoverishment despite greening: A case study from central Senegal. *J. Arid Environ.* **2013**, *90*, 55–66.
79. Schlesinger, W.H.; Reynolds, J.F.; Cunningham, G.L.; Huenneke, L.F.; Jarrell, W.M.; Virginia, R.A.; Whitford, W.G. Biological feedbacks in global desertification. *Science* **1990**, *247*, 1043–1048.
80. Reynolds J.F.; Virginia, R.A.; Kemp, P.R.; De Soyza, A.G.; Tremmel, D.C. Impact of drought on desert shrubs: Effects of seasonality and degree of resource island development. *Ecol. Monogr.* **1999**, *69*, 69–106.
81. Stellmes, M.; Udelhoven, T.; Röder, A.; Sonnenschein, R.; Hill, J. Dryland observation at local and regional scale—Comparison of Landsat TM/ETM+ and NOAA AVHRR time series. *Remote Sens. Environ.* **2010**, *114*, 2111–2125.
82. Röder, A.; Udelhoven, T.; Hill, J.; del Barrio, G.; Tsiourlis, G. Trend analysis of Landsat-TM and ETM+ imagery to monitor grazing impact in a rangeland ecosystem in Northern Greece. *Remote Sens. Environ*. **2008**, *112*, 2863–2875.
83. Lasanta, T.; Vicente-Serrano, S.M. Complex land cover change processes in semiarid Mediterranean regions: An approach using Landsat images in northeast Spain. *Remote Sens. Environ.* **2012**, *124*, 1–14.

84. Peñuelas, J.; Gordon, C.; Llorens, L.; Nielsen, T.; Tietema, A.; Beier, C.; Bruna, P.; Emmett, B.; Estiarte, M.; Gorissen, A. Nonintrusive field experiments show different plant responses to warming and drought among sites, seasons, and species in a north-south European gradient. *Ecosystems* **2004**, *7*, 598–612.
85. Maselli, F.; Cherubinib, P.; Chiesia, M.; Gilabert, M.A.; Lombardie, F.; Moreno, A.; Teobaldellid, M.; Tognettie, R. Start of the dry season as a main determinant of inter-annual Mediterranean forest production variations. *Agric. For. Meteorol.* **2014**, *194*, 197–206.
86. Hielkema, J.U.; Prince, S.D.; Astle, W.L. Rainfall and vegetation monitoring in the savanna zone of the democratic-republic of Sudan using the NOAA advanced very high-resolution radiometer. *Int. J. Remote Sens.* **1986**, *7*, 1499–1513.
87. Justice, C.O.; Hiernaux, P.H.Y. Monitoring the grasslands of the Sahel using NOAA-AVHRR data. Niger, 1983. *Int. J. Remote Sens.* **1986**, *7*, 1475–1497.
88. Sannier, C.A.D.; Taylor, J.C. Real-time vegetation monitoring with NOAA-AVHRR in Southern Africa for wildlife management and food security assessment. *Int. J. Remote Sens.* **1998**, *19*, 621–639.
89. Wang, J.; Price, K.P.; Rich, P.M. Spatial patterns of NDVI response to precipitation and temperature in the central Great Plains. *Int. J. Remote Sens.* **2001**, *22*, 3827–3844.
90. Wessels, K.J.; Prince, S.D.; Frost, P.E.; van Zyl, D. Assessing the effects of human-induced land degradation in the former homelands of northern South Africa with a 1 km AVHRR NDVI time-series. *Remote Sens. Environ.* **2004**, *91*, 47–67.
91. Diouf, A.; Lambin, E.F. Monitoring land-cover changes in semi-arid regions: Remote sensing data and field observations in the Ferlo, Senegal. *J. Arid Environ.* **2001**, *48*, 129–148.
92. Hein, L.; de Ridder, N.; Hiernaux, P.; Leemans, R.; de Witd, A.; Schaepman, M. Desertification in the Sahel: Towards better accounting for ecosystem dynamics in the interpretation of remote sensing images. *J. Arid Environ.* **2011**, *75*, 1164–1172.
93. Breshears, D.D. Adams, H.D.; Eamus, D.; McDowell, N.G.; Law, D.J.; Will, R.E.; Williams, A.P.; Zou, C.B. The critical amplifying role of increasing atmospheric moisture demand on tree mortality and associated regional die-off. *Front. Plant. Sci.* **2013**, *4*, doi:10.3389/fpls.2013.00266.
94. Anderegg, W.R.L., Berry J.A.; Smith, D.D.; Sperry, J.S.; Anderegg, L.D.L.; Field, C.B.; The roles of hydraulic and carbon stress in a widespread climate-induced forest die-off. *Proc. Natl. Acad. Sci. USA* **2012**, *109*, 233–237.
95. Eamus, D.; Boulain, N.; Cleverly, J.; Breshears, D.D. Global change-type drought-induced tree mortality: Vapor pressure deficit is more important than temperature per se in causing decline in tree health. *Ecol. Evol.* **2013**, *3*, 2711–2729.
96. Stephenson, N.L. Climatic control of vegetation distribution: The role of the water balance. *Am. Nat.* **1990**, *135*, 649–670.
97. Vicente-Serrano, S.M.; Camarero, J.J.; Azorín-Molina, C. Diverse responses of forest growth to drought time-scales in the northern hemisphere. *Glob. Ecol. Biogeogr.* **2014**, *23*, 1019–1030.
98. Nicholson, S.E.; Davenport, M.L.; Malo, A.R. A comparison of the vegetation response to rainfall in the Sahel and east Africa, using normalized difference vegetation index from NOAA-AVHRR. *Clim. Chang.* **1990**, *17*, 209–241.

99. Santos, P.; Negrín, A.J. A comparison of the normalized difference vegetation index and rainfall for the Amazon and Notheastern Brazil. *J. Climate* **1997**, *36*, 958–965.
100. Farrar, T.J.; Nicholson, S.E.; Lare, A.R. The influence of soil type on the relationships between NDVI, rainfall and soil moisture in semiarid Botswana II: NDVI response to soil moisture. *Remote Sens. Environ.* **1994**, *50*, 121–133.
101. Donohue, R.J.; Roderick, M.L.; McVicar, T.R.; Farquhar, G.D. Impact of CO_2 fertilization on maximum foliage cover across the globe's warm, arid environments. *Geophys. Res. Lett.* **2013**, *40*, 3031–3035.
102. Farquhar, G.D. Carbon dioxide and vegetation. *Science* **1997**, *278*, doi:10.1126/science.278.5342.1411.
103. Higgins, S.I.; Scheiter, S. Atmospheric CO_2 forces abrupt vegetation shifts locally, but not globally. *Nature* **2012**, *488*, 209–212.
104. Smith, S.D.; Huxman, T.E.; Zitzer, S.F.; Charlet, T.N.; Housman, D.C.; Coleman, J.S.; Fenstermaker, L.K.; Seemann, J.R.; Nowak, R.S. Elevated CO_2 increases productivity and invasive species success in an arid ecosystem. *Nature* **2000**, *408*, 79–82.
105. Reich, P.B.; Hobbie, S.A.; Lee, T.D. Plant growth enhancement by elevated CO_2 eliminated by joint water and nitrogen limitation. *Nature Geosci.* **2014**, *7*, 920–924.
106. Begue, A.; Vintrou, E.; Ruelland, D.; Claden, M.; Dessay, N. Can a 25-year trend in Soudano-Sahelian vegetation dynamics be interpreted in terms of land use change? A remote sensing approach. *Glob. Environ. Change* **2011**, *21*, 413–420.
107. Brink, A.B.; Eva, H.D. Monitoring 25 years of land cover change dynamics in Africa: A sample based remote sensing approach. *Appl. Geogr.* **2009**, *29*, 501–512.
108. Reij, C.; Tappan, G.; Belemvire, A. Changing land management practices and vegetation on the Central Plateau of Burkina Faso (1968–2002). *J. Arid Environ.* **2005**, *63*, 642–659.
109. Rasmussen, K.; Fog, B.; Madsen, J.E. Desertification in reverse? Observations from northern Burkina Faso. *Glob. Environ. Change* **2001**, *11*, 271–282.
110. Van Auken, O.W. Shrub invasions of North American Semiarid grasslands. *Annu. Rev. Ecol. Syst.* **2000**, *31*, 197–215.